JGR Planets

RESEARCH ARTICLE

10.1029/2025JE009242

Rock Coatings as Evidence for Late Surface Alteration on the Floor of Jezero Crater, Mars

Bradley J. Garczynski[1], Briony H. N. Horgan[1], Jeffrey R. Johnson[2], Melissa S. Rice[3], Lucia Mandon[4], Baptiste Chide[5], Andreas Bechtold[6,7], Pierre Beck[8], James F. Bell III[9], Erwin Dehouck[10], Alberto G. Fairén[11,12], Felipe Gómez[11], Pierre-Yves Meslin[13], Gerhard Paar[14], Mark A. Sephton[15], Justin I. Simon[16], Christoph Traxler[17], Alicia Vaughan[18], Roger C. Wiens[1], Tanguy Bertrand[19], Olivier Beyssac[20], Adrian J. Brown[21], Emily L. Cardarelli[22], Edward A. Cloutis[23], Louise Duflot[9], David T. Flannery[24], Patrick Gasda[5], Alexander G. Hayes[12], Christopher D. K. Herd[25], Linda Kah[26], Kjartan B. Kinch[27], Nina Lanza[5], Marco Merusi[27], Chase C. Million[28], Jorge I. Núñez[2], Ann M. Ollila[5], Clément Royer[1], Michael St. Clair[28], Christian Tate[12], and Anastasia Yanchilina[29]

[1]Department of Earth, Atmospheric, and Planetary Sciences, Purdue University, West Lafayette, IN, USA, [2]Johns Hopkins University Applied Physics Laboratory, Laurel, MD, USA, [3]Department of Geology, Western Washington University, Bellingham, WA, USA, [4]Division of Geological and Planetary Sciences, California Institute of Technology, Pasadena, CA, USA, [5]Los Alamos National Laboratory, Los Alamos, NM, USA, [6]Austrian Academy of Sciences, Vienna, Austria, [7]Department of Lithospheric Research, University of Vienna, Vienna, Austria, [8]Institut de Planétologie et Astrophysique de Grenoble, CNRS, Université Grenoble Alpes, Grenoble, France, [9]School of Earth and Space Exploration, Arizona State University, Tempe, AZ, USA, [10]Univ Lyon, UCBL, ENSL, UJM, CNRS, LGL-TPE, Villeurbanne, France, [11]Centro de Astrobiología, Consejo Superior de Investigaciones Cientificas-Instituto Nacional de Tecnica Aeroespacial, Madrid, Spain, [12]Department of Astronomy, Cornell University, Ithaca, NY, USA, [13]IRAP, CNRS, UPS, CNES, Université de Toulouse, Toulouse, France, [14]JOANNEUM RESEARCH Forschungsgesellschaft mbH, Institute for Information Technologies, Graz, Austria, [15]Department of Earth Science and Engineering, Imperial College London, London, UK, [16]Center for Isotope Cosmochemistry and Geochronology, Astromaterials Research and Exploration Science, NASA Johnson Space Center, Houston, TX, USA, [17]VRVis Zentrum für Virtual Reality und Visualisierung Forschungs-GmbH, Vienna, Austria, [18]Apogee Engineering, LLC, Flagstaff, AZ, USA, [19]Laboratoire d'Etudes Spatiales et d'Instrumentation en Astrophysique, Observatoire de Paris-PSL, CNRS, Sorbonne Université, Université de Paris Cité, Meudon, France, [20]Institut de Minéralogie, de Physique des Matériaux et de Cosmochimie, CNRS, Sorbonne Université, Muséum National d'Histoire Naturelle, Paris, France, [21]Plancius Reseach, LLC, Severna Park, MD, USA, [22]Jet Propulsion Laboratory, California Institute of Technology, Pasadena, CA, USA, [23]Centre for Terrestrial and Planetary Exploration, University of Winnipeg, Winnipeg, MB, Canada, [24]Queensland University of Technology, Brisbane, QLD, Australia, [25]Department of Earth and Atmospheric Sciences, University of Alberta, Edmonton, AB, Canada, [26]Department of Earth and Planetary Sciences, University of Tennessee, Knoxville, TN, USA, [27]Niels Bohr Institute, University of Copenhagen, Copenhagen, Denmark, [28]Million Concepts, Louisville, KY, USA, [29]Impossible Sensing, St. Louis, MO, USA

Abstract During the NASA *Perseverance* rover's exploration of the Jezero crater floor, coatings were commonly observed on rocks. These features may record past water-rock-atmosphere interactions on the crater floor, and understanding their origin is important for constraining the timing of potential water activity and habitability at Jezero. Here, we characterize the morphologic, chemical, and spectral properties of the crater floor rock coatings using color images, visible/near-infrared reflectance spectra, and chemical data from the Mastcam-Z and SuperCam instruments. We show that coatings are common and compositionally similar across the crater floor, and consistent with a mixture of dust, fine regolith, sulfates, and ferric oxides indurated as a result of one or more episodes of widespread surface alteration. All coatings exhibit a similar smooth homogenous surface with variable thickness, color, and spatial extent on rocks, likely reflecting variable oxidation and erosional expressions related to formation and/or exposure age. Coatings unconformably overlie eroded natural rock surfaces, suggesting relatively late deposition that may represent one of the last alteration episodes on the Jezero crater floor. While more common at Jezero, these coatings may be consistent with rock coatings previously observed in situ at other landing sites and may be related to duricrust formation, suggesting a global alteration process on Mars that is not unique to Jezero. The *Perseverance* rover likely sampled these rock coatings on the crater floor and the results from this study could provide important context for future investigations by the Mars Sample Return mission aimed at constraining the geologic and alteration history of Jezero crater.

Key Points:

- Rock coatings are common across the Jezero crater floor and likely represent relatively late and widespread surface alteration
- Composition is consistent with a variable mixture of dust, fine regolith, sulfates, and ferric oxides cemented during past water interaction
- Future sample return studies could further investigate potentially sampled coatings to constrain the alteration history of Jezero crater

Supporting Information:

Supporting Information may be found in the online version of this article.

Correspondence to:

B. J. Garczynski,
bradleygarczynski@gmail.com

Citation:

Garczynski, B. J., Horgan, B. H. N., Johnson, J. R., Rice, M. S., Mandon, L., Chide, B., et al. (2025). Rock coatings as evidence for late surface alteration on the floor of Jezero crater, Mars. *Journal of Geophysical Research: Planets*, *130*, e2025JE009242. https://doi.org/10.1029/2025JE009242

Received 2 JUL 2025
Accepted 16 JUL 2025

Author Contributions:

Conceptualization: Bradley J. Garczynski, Briony H. N. Horgan
Data curation: Bradley J. Garczynski
Formal analysis: Bradley J. Garczynski, Baptiste Chide, Andreas Bechtold, Gerhard Paar, Christoph Traxler
Funding acquisition: Briony H. N. Horgan, James F. Bell III
Investigation: Bradley J. Garczynski, Briony H. N. Horgan, Jeffrey R. Johnson, Melissa S. Rice, Lucia Mandon, Baptiste Chide, Andreas Bechtold, Pierre Beck, James F. Bell III, Erwin Dehouck, Alberto G. Fairén, Felipe Gómez, Pierre-Yves Meslin, Gerhard Paar, Mark A. Sephton, Justin

I. Simon, Christoph Traxler, Alicia Vaughan, Roger C. Wiens, Tanguy Bertrand, Olivier Beyssac, Adrian J. Brown, Emily L. Cardarelli, Edward A. Cloutis, Louise Duflot, David T. Flannery, Patrick Gasda, Alexander G. Hayes, Christopher D. K. Herd, Linda Kah, Kjartan B. Kinch, Nina Lanza, Marco Merusi, Chase C. Million, Jorge I. Núñez, Ann M. Ollila, Clément Royer, Michael St. Clair, Christian Tate, Anastasia Yanchilina
Methodology: Bradley J. Garczynski, Briony H. N. Horgan
Software: Chase C. Million, Michael St. Clair
Supervision: Briony H. N. Horgan
Visualization: Bradley J. Garczynski, Lucia Mandon, Baptiste Chide, Andreas Bechtold, Gerhard Paar, Christoph Traxler
Writing – original draft: Bradley J. Garczynski
Writing – review & editing: Bradley J. Garczynski, Briony H. N. Horgan, Jeffrey R. Johnson, Melissa S. Rice, Lucia Mandon, Pierre Beck, Mark A. Sephton, Justin I. Simon, Alicia Vaughan, Roger C. Wiens, Tanguy Bertrand, Emily L. Cardarelli, Linda Kah

Plain Language Summary The NASA *Perseverance* rover spent the first Earth year of its mission exploring the floor of Jezero crater on Mars to investigate geology, search for signs of past life, and collect samples for future return to Earth. Rock coatings were commonly observed by the rover and may record important information regarding past water activity and habitability at Jezero. In this study, we used images and remote sensing data from the Mastcam-Z and SuperCam instruments to describe the distribution, surface expressions, and composition of the coatings. We find that coatings occur and are compositionally similar throughout the crater floor, and may have formed during one or more of the most recent episodes of alteration activity on the Jezero crater floor. While coatings seem more common at Jezero, these features may be similar to rock coatings previously identified at other rover landing sites on Mars, suggesting that coating formation is a global process that is not unique to Jezero. The *Perseverance* rover likely collected some of this coating material in rock samples that NASA plans to return to Earth; thus, this work will provide important context for future sample studies investigating these features to better understand Jezero's geologic and surface alteration history.

1. Introduction

After touching down on Mars at the Octavia E. Butler landing site on 18 February 2021, the NASA Mars 2020 *Perseverance* rover began its exploration of Jezero crater to characterize regional geology, identify habitable paleoenvironments, seek signs of ancient life, and collect geologically diverse rock and regolith samples for return to Earth by future missions (Farley et al., 2020). At Jezero, *Perseverance* is investigating the ~45-km-diameter Noachian-aged impact crater and an ancient fluviolacustrine system (Fassett & Head, 2005; Schon et al., 2012) that was active in the late Noachian and possibly Hesperian (Mangold et al., 2020; Salese et al., 2020). The crater exhibits numerous geomorphic and mineralogical indicators of its watery past, including multiple sedimentary fans interpreted as at least partially deltaic that are connected to an extensive valley network (Goudge et al., 2017, 2018; Mangold et al., 2021), as well as orbital (Brown et al., 2020; Ehlmann et al., 2008; Goudge et al., 2012; Horgan, Anderson, et al., 2020; Horgan, Johnson, et al., 2020; Tarnas et al., 2019; Zastrow & Glotch, 2021) and in situ (Clavé et al., 2023; Farley et al., 2022; Mandon et al., 2023; Scheller et al., 2022; Tice et al., 2022; Wiens et al., 2022) detections of secondary alteration minerals. Despite this resounding evidence, the timing, style, and frequency of alteration events within Jezero crater remains poorly constrained and a topic of ongoing investigations.

During the mission's first science campaign investigating the floor of Jezero crater (Sun et al., 2023), the *Perseverance* rover commonly observed apparent coatings on the eroded natural surfaces of crater floor rocks (Figures 1 and 2). These surface features occurred in both crater floor units investigated by the *Perseverance* rover: the Máaz (Navajo word for "Mars") formation, a cratered pyroxene-bearing terrain interpreted to represent a series of ancient lava flows (Horgan et al., 2023; Udry et al., 2023), and the Séítah (Navajo word for "amidst the sand") formation, a stratigraphically older ridged and dune-filled landscape interpreted as an olivine-rich cumulate (Beyssac et al., 2023; Liu et al., 2022). The presence of these features on modern rock surfaces may suggest weathering processes that occurred after the most recent exhumation of the crater floor (Bishop et al., 2002; Mandon et al., 2023), which likely experienced multiple episodes of burial and erosion (Horgan et al., 2023; Quantin-Nataf et al., 2023). Some of these coatings were likely sampled by the *Perseverance* rover and their future investigations in laboratories on Earth may help elucidate the timing of past alteration activity and exhumation of the Jezero crater floor (Simon et al., 2023).

Evidence of chemical surface alteration, including rock coatings and weathering rinds, can provide an important record of the duration and nature of past surface environments, and have previously been identified as key targets for investigation and sampling at Jezero (Beaty et al., 2019). Weathering processes can modify rock compositions through aqueous alteration by adding material to produce coatings or removing material from the host rock through mineral dissolution (Lanza et al., 2015). Alternative anhydrous hypotheses for coatings involve volcanic vapor precipitates (Schmidt et al., 2024). Coatings typically occur unconformably on rock surfaces and can form due to microbial activity (Northup et al., 2010; Parchert et al., 2012; Viles, 1995) or abiotically through the cementation of dust, clays, metals, or other mobile element species to rock surfaces (Dorn, 2009; Salvatore et al., 2013). In contrast, weathering rinds are typically continuous with the underlying rock and represent a chemical gradient with a composition similar to the host rock but depleted in certain mobile elements (Salvatore et al., 2013;

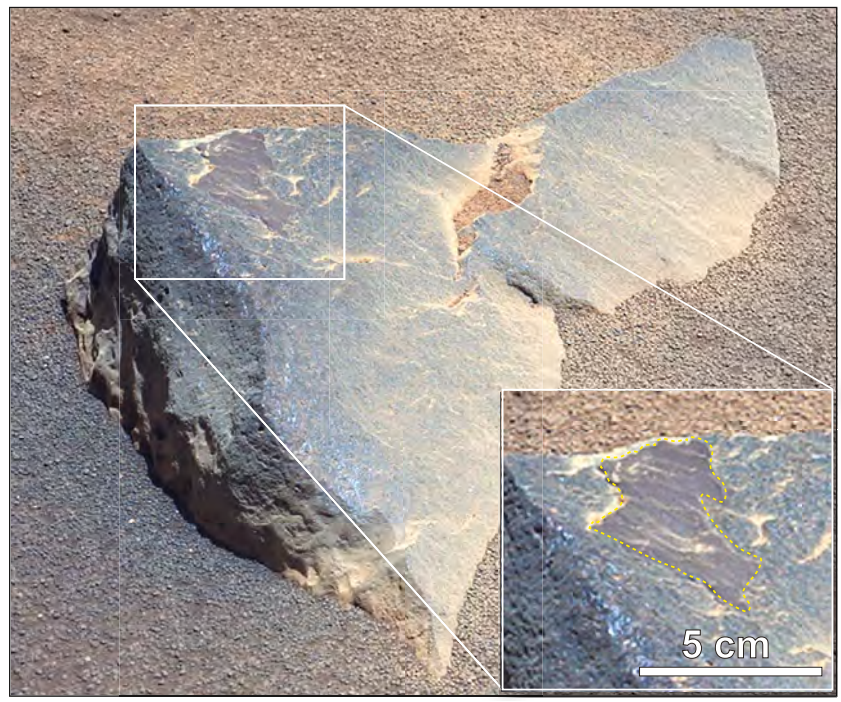

Figure 1. Mastcam-Z left eye enhanced color red/blue/green image (zcam08102) acquired on sol 56 showing a potential purple-hued surface coating (outlined by yellow dashed line) on a crater floor rock within the Máaz formation.

Smith et al., 2017). Despite their different formation mechanisms, both coatings and rinds can form in the same environment and record important information about past climate and weathering conditions such as the amount and type of fluids that were present (Minitti et al., 2007; Perry & Sephton, 2006). In addition to recording information about past alteration, these features can also provide suitable habitats for microbes and record evidence of past life (Krinsley et al., 2009; Kuhlman et al., 2008; Wierzchos et al., 2011). On Mars, these microenvironments could have shielded microbes from harmful surface radiation and thus may provide compelling targets for biosignature detection (Marnocha, 2017).

In this study, we investigated the spectral and textural properties of rock coatings on the crater floor to better inform hypotheses regarding the alteration history of Jezero. In particular, we focused on characterizing the morphology, distribution, and composition of these surface features using in situ rover observations including Mastcam-Z color images and visible and near-infrared (VNIR; 422–1,022 nm) multispectral data. Mastcam-Z observations were supported by compositional data from SuperCam visible and short-wave infrared reflectance spectra (VISIR; 0.40–0.85 μm and 1.3–2.6 μm), elemental chemistry from SuperCam laser-induced breakdown spectroscopy (LIBS), as well as fine-scale textural properties from high-resolution color images using the WATSON camera on the rover's arm. In addition, we conducted a first order comparison of the Jezero crater floor coatings with coatings previously observed by in situ rover missions at other Mars landing sites to investigate a potential relationship in formation mechanisms. The aim of this work was to better constrain the timing and nature of alteration activity at Jezero crater and identify potential habitable paleoenvironments. The results of this work provide important context for additional coating observations and analyses at Jezero as well as a framework for future Mars Sample Return studies.

2. Methods

2.1. Instrumentation

2.1.1. Mastcam-Z

The Mast Camera Zoom (Mastcam-Z) imaging system on board the *Perseverance* rover is a pair of zoomable, focusable, 1,648 × 1,214 pixel charge-coupled device (CCD) cameras that allows for high resolution,

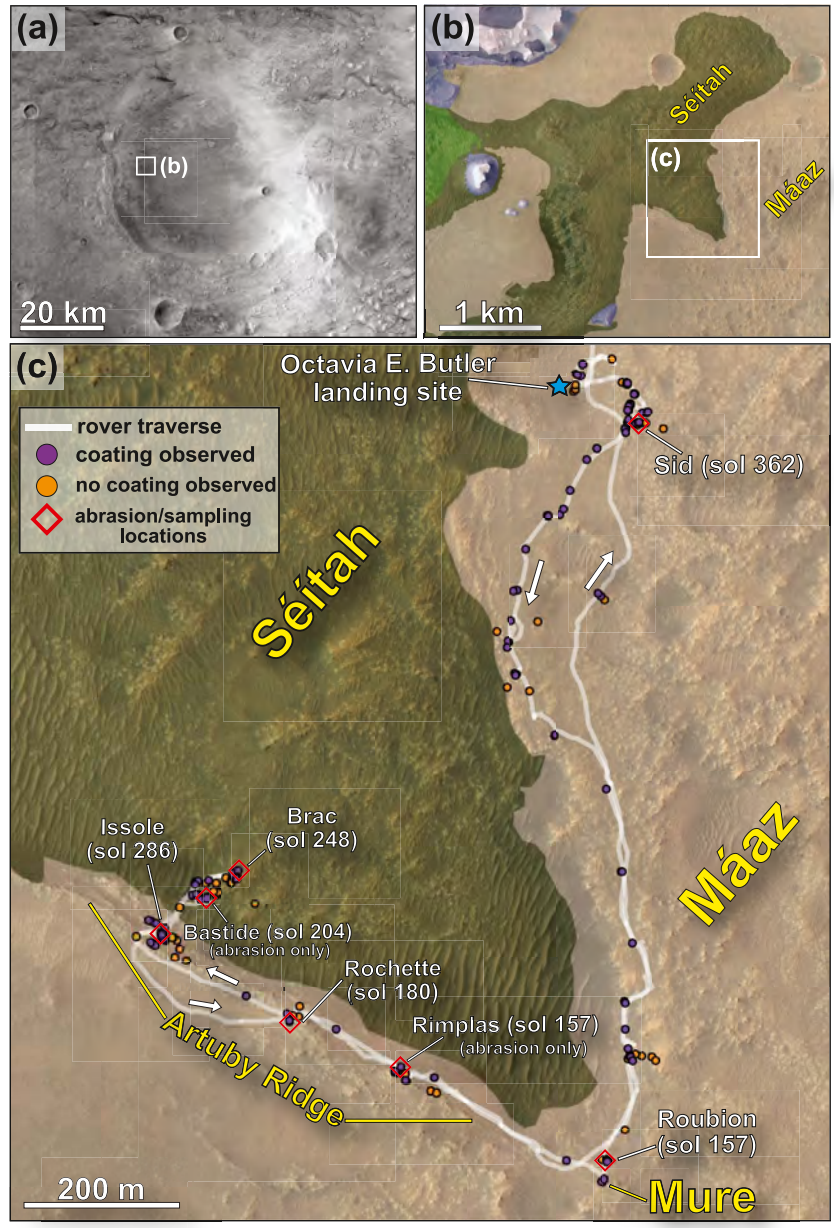

Figure 2. Overview of Jezero crater floor from orbital images. (a) CTX mosaic of Jezero crater. (b) HiRISE approximate true-color mosaic of the crater floor overlain by geologic map from Stack et al. (2020) showing the Máaz (beige) and Séítah (green) formations. (c) Region investigated during the Crater Floor campaign showing rover traverse and notable locations. Colored dots represent locations of all nearfield (<10 m away) and midfield (10–50 m) rock targets investigated by the Perseverance rover on the crater floor. Purple dots represent rock targets that appeared coated in Mastcam-Z and/or SuperCam images, while orange dots correspond to rock targets without visible coatings as determined by this study. Sol numbers noted next to abrasion/sampling locations refer to the sol of arrival at that workspace.

multispectral, and stereoscopic imaging of Jezero crater (Bell et al., 2021, 2022). Mounted ~2 m above the surface on *Perseverance's* Remote Sensing Mast, each camera is equipped with broadband Bayer red/blue/green (RGB) filters bonded to the CCD and an eight-position filter wheel for multispectral observations. Each filter wheel includes one broadband IR-cutoff filter to acquire standard Bayer RGB color images, six narrowband VNIR filters, and one solar imaging filter. Mastcam-Z builds upon the heritage of previous Mars rover multispectral imagers (Bell et al., 2003) and is similar to the Mastcam instrument (Bell et al., 2017) operating on board the Mars Science Laboratory (MSL) *Curiosity* rover at Gale crater, with additional zoom capabilities and a modified filter

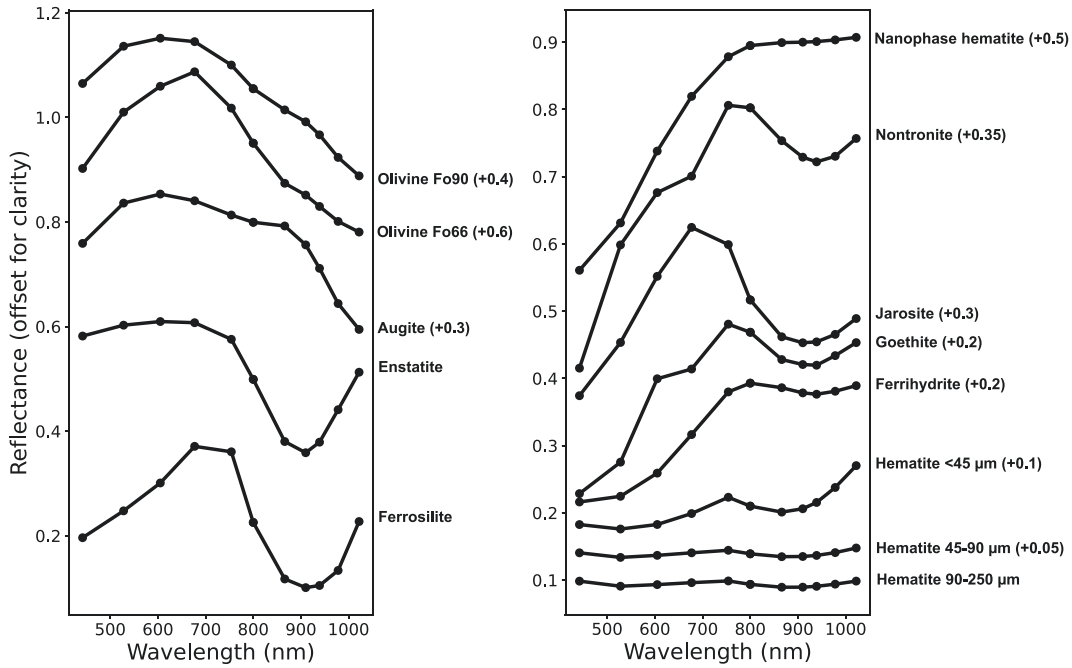

Figure 3. Laboratory reflectance spectra of ferrous primary (left) and ferric secondary (right) minerals convolved to Mastcam-Z spectral bandpasses. Spectra are stacked for clarity and amounts of offset are noted next to mineral names. The sources of laboratory spectra are detailed in Table S3 of Rice et al. (2023). Spectra of hematite <45, 45–90, and 90–250 μm are from the University of Winnipeg Spectrophotometer Facility and from samples HEM103_0, HEM103_2, HEM103_4, respectively.

set. The focal lengths of each camera can vary between 26 mm ("Z26") and 110 mm ("Z110"), allowing for variable fields of view. At maximum focal length, the cameras can resolve ∼0.7 mm features (≥5 pixels in size) in the nearfield (∼2 m) and ∼3.3 cm features at 100 m distance. In addition to the three broadband RGB filters, the cameras together cover 11 distinct wavelengths between 442 and 1,022 nm. These zoom and multispectral capabilities allow Mastcam-Z to investigate fine-scale textures and outcrop stratigraphy, and provide a preliminary assessment of color and mineralogical variability along the rover's traverse. The data also help the science team identify targets for sampling and more detailed chemical and textural analyses with arm-mounted proximity science instruments.

Preflight calibration measurements were used to convert raw Mastcam-Z images to radiance as described in Hayes et al. (2021). To account for local changes in illumination conditions as a result of time of year, time of day, and atmospheric conditions (e.g., dust loading, clouds, etc.), two deck mounted radiometric calibration targets were imaged at similar times to each multispectral observation acquired on Mars. Measurements from these calibration targets were then used to convert image data from radiance to units of relative reflectance (e.g., *R**, I/F) (Kinch et al., 2020; Merusi et al., 2022).

While Mastcam-Z was not designed as a spectrometer, the spectral range (422–1,022 nm) of the instrument is useful for distinguishing ferrous (Fe^{2+}) primary minerals and ferric (Fe^{3+}) secondary alteration products (Figure 3). High and low calcium pyroxenes can be distinguished from the position of the ferrous crystal field absorption near 1,000 nm, as lower calcium content tends to shift the broad absorption band to shorter wavelengths (Cloutis & Gaffey, 1991). Olivine exhibits a broader 1,000 nm absorption with a long near infrared (NIR) slope and a spectral peak at or below 700 nm that is sensitive to grain size and Mg/Fe content (Adams, 1975; Cloutis et al., 1986). Fe^{3+}-bearing minerals (e.g., iron oxides, oxyhydroxides, sulfates, phyllosilicates) also exhibit distinctive absorption features, including crystal field bands near 800–1,000 nm and a strong charge transfer band near 400–500 nm that extends into the ultraviolet (Morris et al., 1985, 1993; Sherman et al., 1982). The strong ferric iron absorptions at shorter wavelengths cause steep positive slopes towards longer wavelengths and a spectral peak around 750 nm. This slope is steeper in spectra of brighter and redder surfaces, typically exhibited by Martian rocks with thick dust cover. Absorptions near 528 nm in Mastcam-Z spectra are consistent

with ferric oxides and are typically used to assess the degree of oxidation of various rock and regolith surfaces. While crystalline and nanophase hematite both exhibit the strong charge transfer band at shorter wavelengths, the latter can be distinguished by the lack of the longer wavelength absorption band centered near 860 nm (Horgan, Anderson, et al., 2020; Horgan, Johnson, et al., 2020). In addition to the sensitivity to iron-bearing phases, the Mastcam-Z spectral range also includes a weak H_2O vibrational overtone/combination band near 950–1,000 nm that is present in certain hydrated minerals (Rice et al., 2010; Wang et al., 2008).

2.1.2. SuperCam

SuperCam is a remote-sensing instrument capable of several techniques including LIBS, VISIR reflectance spectroscopy, remote time-resolved Raman spectroscopy, acoustic recording, and high-resolution imaging via its Remote Micro-Imager (RMI) (Maurice et al., 2021; Wiens et al., 2021). All of the SuperCam techniques are co-boresighted and use rasters (1 × 5, 1 × 10, 2 × 2, or 3 × 3 patterns) to observe multiple points on each target.

SuperCam's LIBS observations and data analyses follow the approach of the ChemCam instrument on the Curiosity rover (Maurice et al., 2012; Wiens et al., 2012). On SuperCam, the LIBS uses a pulsed laser beam focused onto a 250–350 μm spot, depending on target distance, to create a brief plasma that emits light containing atomic emission peaks from the elements present in the target. Normally, 30 laser shots and 30 spectra are obtained at each point; however, depth profiles of up to 150 laser shots have been performed. The penetration depth per shot depends strongly on the surface hardness and its reflectance at the laser wavelength, but is roughly on the order of 1 μm per shot. Especially in the case of depth profiles, the shot-to-shot compositional trends can be observed as a function of laser pulse number as a proxy for depth. However, most analyses use a simpler process in which the first five spectra are discarded to avoid dust contamination, and elemental compositions are determined after averaging the remaining spectra from a given observation point. Data treated in this way have been calibrated against a large library of standards to provide quantitative abundances for eight major elements quantified as oxides: SiO_2, TiO_2, Al_2O_3, FeO_T, MgO, CaO, Na_2O, and K_2O, where the total iron is quantified as a single oxidation state since LIBS does not distinguish between oxidation states. The algorithms and the error analyses are given in Anderson et al. (2022).

SuperCam's VISIR observations cover the spectral range from 0.4 to 2.6 μm with a gap between 0.46–0.54 and 0.85–1.3 μm. The gaps and spectral ranges of SuperCam VISIR are dictated by the spectral ranges of the focal plane arrays used for LIBS and Raman measurements (Wiens et al., 2021). The visible range uses the same spectrometers as the LIBS technique using averages of 50 spectra at each point. The near infrared spectral range is collected using an acousto-optic tunable filter to scan the wavelengths over 256 channels (resolution of 32 cm^{-1}) by varying the radio frequency provided to a tellurium dioxide crystal. The field of view of the visible-range spectrometers is 0.85 mrad, while the infrared field of view is substantially larger, at 1.15 mrad. The infrared spectrometer design and operation is described in Fouchet et al. (2022). Radiance calibration of the respective visible and infrared spectrometers is described in Legett et al. (2022) and Royer et al. (2023).

SuperCam RMI images were taken through the instrument's telescope using a 2,048 × 2,048 pixel CMOS sensor equipped with a Bayer filter to provide RGB color (Maurice et al., 2021). The images subtend an angular space of 18.8 mrad and have an effective resolution of ∼40 μrad (∼120 μm at 3 m observation distance). Images were corrected to approximate true color based on calibration with RGB targets onboard the rover or presented in enhanced color using a Gaussian stretch algorithm. Due to substantial vignetting, the corners of the image were masked and flat-fielded. Several images were taken during rasters, from which mosaics were produced.

2.1.3. WATSON

The Wide Angle Topographic Sensor for Operations and eNgineering (WATSON) is a microscopic imager mounted on the arm of the *Perseverance* rover. As part of the Scanning Habitable Environments with Raman and Luminescence for Organics and Chemicals (SHERLOC) instrument, the camera is nearly identical to the Mars Hand Lens Imager (Edgett et al., 2012, 2015) onboard the MSL *Curiosity* rover and is used to investigate fine-scale textures of rock, regolith, and dust (Bhartia et al., 2021; Minitti et al., 2021). WATSON also supports arm placement for SHERLOC and the Planetary Instrument for X-ray Lithochemistry (PIXL) instrument and provides color context imaging for organic and mineralogical data acquired by SHERLOC and elemental maps generated by PIXL. Additionally, WATSON provides engineering support to assist in sample and caching activities (Moeller et al., 2020) and also monitor the ongoing health and condition of rover components. The camera

collects color images via a Bayer pattern over a 1,640 × 1,214 pixel CCD and is focusable at a variety of working distances from 1.78 cm (~13 μm/pixel) to infinity, allowing WATSON to resolve down to silt-sized grains (Bhartia et al., 2021; Edgett et al., 2019).

2.2. Distribution, Morphology, and Texture

To assess the distribution of rock coatings across the Jezero crater floor, we reviewed all Mastcam-Z (Bayer filter and multispectral) and SuperCam RMI images acquired of 256 nearfield (<10 m away) and midfield (10–50 m away) rock targets investigated by the *Perseverance* rover between sols 0 and 379. A full list of targets and associated metadata is archived and available in Garczynski (2025). We excluded images that did not cover natural rock surfaces, such as regolith observations and SuperCam RMI images of abrasion patches. Enhanced color images were used to better highlight the color differences and more easily distinguish a surface coating from the underlying rock. If Mastcam-Z multispectral data were available for a given rock target, we analyzed both enhanced color and decorrelation stretch (DCS; Gillespie et al., 1986) composites using 754 nm (L2), 528 nm (L5), 442 nm (L6) filter images (referred to as "L256 DCS") as we determined these composites best highlight the coatings. For each rock target, we noted whether or not we observed obvious evidence of a coating within the images, including surfaces that exhibited color and/or textural differences with the underlying rock. To quantify the distribution of coatings, we calculated the percentage of total rock targets that showed clear evidence of coatings within the Máaz and Séítah formations as well as a total percentage across the entire crater floor. We note the limitations of this method as in some cases the coatings may have been obscured by a layer of surface dust. To better understand the distribution of coatings around the *Perseverance* rover within a given area on the crater floor, we also analyzed 16 nearfield and midfield z110 Bayer filter enhanced color RGB landscape mosaics acquired at various locations along the crater floor traverse (Table S1 in Supporting Information S1).

Texture and morphology of the coatings was also assessed using Mastcam-Z and Supercam RMI images in addition to WATSON images. We note that this study did not conduct a comprehensive analysis of all available WATSON images of crater floor rock targets but rather used a few representative images of coatings to provide information on fine scale morphology and texture. For each coating identified, we qualitatively assessed the apparent color, thickness, texture, and spatial extent on the rock surface. To more quantitatively assess the thickness, areal coverage, and geometry of coatings, we generated three-dimensional models using Mastcam-Z stereo images with PRo3D software and methods described in Paar et al. (2023). An animation of coatings generated using the Pro3D software is presented in Movie S1. In addition to the PRo3D analysis, data from a SuperCam LIBS depth profile on a rock coating at target Chokecherry (Sol 378, Máaz fm.) was also used to estimate the coating thickness.

2.3. Spectral and Chemical Properties

2.3.1. Mastcam-Z Multispectral

Representative spectra were extracted by averaging R^* values of pixels within regions of interest (ROIs) selected for each Mastcam-Z calibrated observation as described by Rice et al. (2023) and archived in a database along with image metadata and composite images (natural color, enhanced color and DCS) (Rice et al., 2022). Coating ROIs were evaluated initially using L256 enhanced color and DCS composite images. For this study, we focused our spectral analysis on 32 nearfield and midfield observations that exhibited the clearest examples of coatings (Garczynski, 2025). To determine any spectral differences between coating morphologies, we assigned each coating ROI with a morphological type (*purple patch*, *continuous*, *thick coating*). Coating spectra were compared to spectra of other representative surfaces including non-coated bedrock, dust, and fine-grained regolith (<500 μm grain size; Vaughan et al., 2023). To further classify spectral variability and quantify potential compositional differences, we used a set of spectral parameters described in Rice et al. (2023) and listed in Table 1.

2.3.2. SuperCam VISIR

SuperCam collected more than 2000 VISIR spectra during the Crater Floor Campaign on a variety of rock and regolith targets (Mandon et al., 2023). To investigate the spectral properties of the coatings in the SuperCam wavelength range, we identified 29 individual point spectra acquired from coated rock surfaces. We excluded spectra with clear signs of saturation, shadowing, and non-coated surfaces within the field of view to avoid

Table 1
List of Reflectance Spectral Parameters Used in This Study

Instrument	Parameter name	Formula	Sensitivity
Mastcam-Z	754 nm (L2)/ 442 nm (L6)	R^*_{754}/R^*_{442}	"Red/blue ratio"; higher values indicate redder material and are consistent with higher degrees of oxidation
	528 nm (L5) band depth	$1 - R^*_{528}/(0.634R^*_{442} + 0.366R^*_{677})$	Larger values consistent with Fe oxidation (Farrand et al., 2008; Morris et al., 1985)
	800 nm (R1)/ 978 nm (R5)	R^*_{800}/R^*_{978}	Large positive values used to indicate broad Fe absorptions in the NIR; values close to 1.0 consistent with phases spectrally neutral in NIR (e.g., sulfates); Small values consistent with hematite (Rice et al., 2023)
	910 nm (R3) band depth	$1 - R^*_{910}/(0.505R^*_{800} + 0.495R^*_{1022})$	Useful to indicate the presence or absence of Fe absorptions in the NIR. Higher values are consistent with low-Ca pyroxene or crystalline ferric materials (Farrand et al., 2008)
Supercam	545 nm band depth	$1 - R_{545}/(0.324R_{430} + 0.676R_{600})$	Crystalline ferric materials
	1,930 nm band depth	$1 - R_{1930}/(0.667R_{1820} + 0.333R_{2150})$	H_2O

spectral mixing. The selected spectra were categorized based on morphology and averaged to obtain a representative spectrum for each coating type. To understand the potential relationship between the coatings and other representative surfaces, we compared the average coating spectra to the average spectra of Jezero dust, fine soil, and both uncoated Máaz and Séítah bedrock as presented in Mandon et al. (2023). To further quantify spectral differences, we used a set of spectral parameters including 545 and 1,930 nm band depth as listed in Table 1. These parameters allowed us to investigate the potential variability in ferric content and degree of hydration, respectively. The RMI images and VISIR footprints of the coating targets can be found in Figure S1 in Supporting Information S1.

2.3.3. SuperCam LIBS

To investigate the chemical properties of the crater floor coatings, we identified 68 LIBS points over coated targets that were analyzed at a distance smaller than 6.5 m. We excluded points that were close to the edge of a coating or where the total laser pulses appeared to penetrate through the coating, revealing the underlying bedrock to avoid contamination from non-coated surfaces. For each point, we averaged major-element oxides composition (MOC) data from shots #6–30 and discarded the first five shots to avoid dust contamination. Each point was categorized based on the geologic formation of the rock target and morphology of the coating. We derived molar compositions from the MOC data and plotted them in Si + Al/Fe + Mg/Ca + Na + K and Mg/Ca/Fe ternary diagrams to better assess the chemical composition of the coatings. To investigate the chemical relationship between coatings and non-coated surfaces, we compared the coating points with LIBS data obtained from bedrock, dust, and fine regolith. Mean dust composition was obtained by averaging data from all the first LIBS shots acquired during the Crater Floor Campaign as described by Lasue et al. (2023). To compare with fine-grained regolith, we used average MOC data of "disturbed soils" reported by Hausrath et al. (2023). The RMI images and LIBS footprints of the coating targets can be found in Figure S1 in Supporting Information S1. To constrain potential thickness and chemical variability within the coatings, we analyzed a LIBS depth profile acquired on target *Chokecherry*. Major-element oxides composition data of MgO, Al_2O_3, FeOT, and Na_2O obtained from 150 individual LIBS shots over a coating were compared to the composition of LIBS shots from a non-coated natural surface on the same rock.

3. Results

3.1. Distribution, Morphology, and Texture

Our assessment of Mastcam-Z and SuperCam RMI images revealed that coatings commonly occurred on crater floor rocks in both the Máaz and Séítah formations and across multiple stratigraphic members (Sun et al., 2023). Of the 256 crater floor rock targets we analyzed, ~62% (n = 158) of these targets exhibited clear evidence of coatings in the images (Figure 2 and Figure S2 in Supporting Information S1). We did not observe major differences in coating distribution between the Máaz and Séítah formations as ~64% (99 out of 155 total) of Máaz rock targets and ~58% (59 out of 101) of Séítah rock targets appeared coated. The percentages we report here are likely lower constraints, as many of the targets on which we did not observe conclusive evidence of coatings

Table 2
Summary of Coating Morphologic Classes Observed on the Jezero Crater Floor

Coating type	Color	Occurrence	Areal extent	Thickness	Distribution on Jezero crater floor
Purple patches (Figures 4–6)	Purple/dark red	Commonly observed on relatively dust-free natural surfaces, especially those cleared by adjacent abrasion activities or SuperCam LIBS laser shots	Discontinuous; typically occurred in isolated patches a few mm to cm across[a]	Appeared variable; likely less than ~300 μm	Observed in both Máaz and Séítah formations
Continuous coatings (Figures 7 and 8)	Variable; gray to muted purple	Typically observed on lower lying surfaces near regolith; occasionally associated with loose, eroded flakes on regolith	More extensive and continuous along rock surface than *purple patches*; a few 10s of cm across[a]	Appeared variable; likely less than ~300 μm	Observed in both Máaz and Séítah formations
Thick coatings (Figures 9 and 10)	Variable; gray to muted purple	Raised, protruding expression; typically observed on the sides or undersides of rocks	Typically ~3–10 cm across[a]	~1–20 mm	Only observed along steeper exposures of Mure and Artuby ridge

[a]Measured across longest axis.

exhibited thick dust cover or were too far to resolve coatings that potentially may have been present on a finer scale. In our analysis of Mastcam-Z enhanced color mosaics, we consistently identified the presence of coated rock surfaces in the vicinity of the rover at multiple locations, further indicating their widespread occurrence. We did not observe obvious signs of coatings at the outcrop scale on some rocks that exhibited extensive evidence of wind abrasion and erosion, possibly due to previous removal of coatings.

Here we describe three morphologic classes of crater floor coatings, discussed in more detail below and summarized in Table 2: (a) *purple patches*, (b) *continuous coatings*, and (c) *thick coatings*. These classifications were defined by qualitatively assessing color, apparent thickness, and spatial extent on rock surfaces in images of crater floor coatings. All observed coatings exhibit a texturally smooth, homogenous surface distinct from the underlying rock and are typically observed on eroded and weathered surfaces.

3.1.1. Purple Patches

Discontinuous patches of coatings were predominantly observed on relatively dust free surfaces in both the Máaz and Séítah formations and typically exhibited purple hues in enhanced color and DCS composite images and purple to dark red hues in natural color images (Figures 1 and 4–6). In some cases, the color of coatings appeared more muted or grayer although such differences often varied with lighting conditions where the purple was more apparent at lower phase angles (Johnson et al., 2022). The patches were especially apparent on natural rock surfaces that were dust-cleared by adjacent abrasion activities (Moeller et al., 2020; Figure 4b and Figure S3 in Supporting Information S1) or laser shots from SuperCam LIBS (Figure 4c). *Purple patches* were absent within all abraded patches but commonly occurred on the adjacent natural surfaces where the thin layer of dust was cleared by the Gas Dust Removal Tool (gDRT) (Moeller et al., 2020). *Purple patches* typically occurred discontinuously, exhibited variable thicknesses and areal coverage on rock surfaces, and occasionally were confined to lower-relief facets in wind-abraded flutes (Figure 5b). Some coatings disturbed by abrasion activities appeared to have fractured along potential layers that may represent distinct episodes of coating formation (Figure S3b in Supporting Information S1). Mastcam-Z PRo3D analysis of *purple patches* indicated that the thicknesses were below the grid size of the model, suggesting a thickness less than ~300 μm. In some cases, especially on higher standing wind abraded boulders, *purple patches* were not apparent at the outcrop scale, but closer inspection with WATSON revealed that these surface features were present at small scales (Figure 6; Wogsland et al., 2023). In some WATSON images, we observed *purple patches* beneath a thin layer of cohesive dust that was easily removed by LIBS shots (Figure 6d). Individual grains within the coatings were not resolvable within the highest resolution images of the *purple patches* (4 cm standoff at 21.7 ± 0.4 μm/pixel; Figure 6e), suggesting a grain size below ~21 μm. Occasionally the *purple patches* were thin enough to be punctured through by the

10.1029/2025JE009242

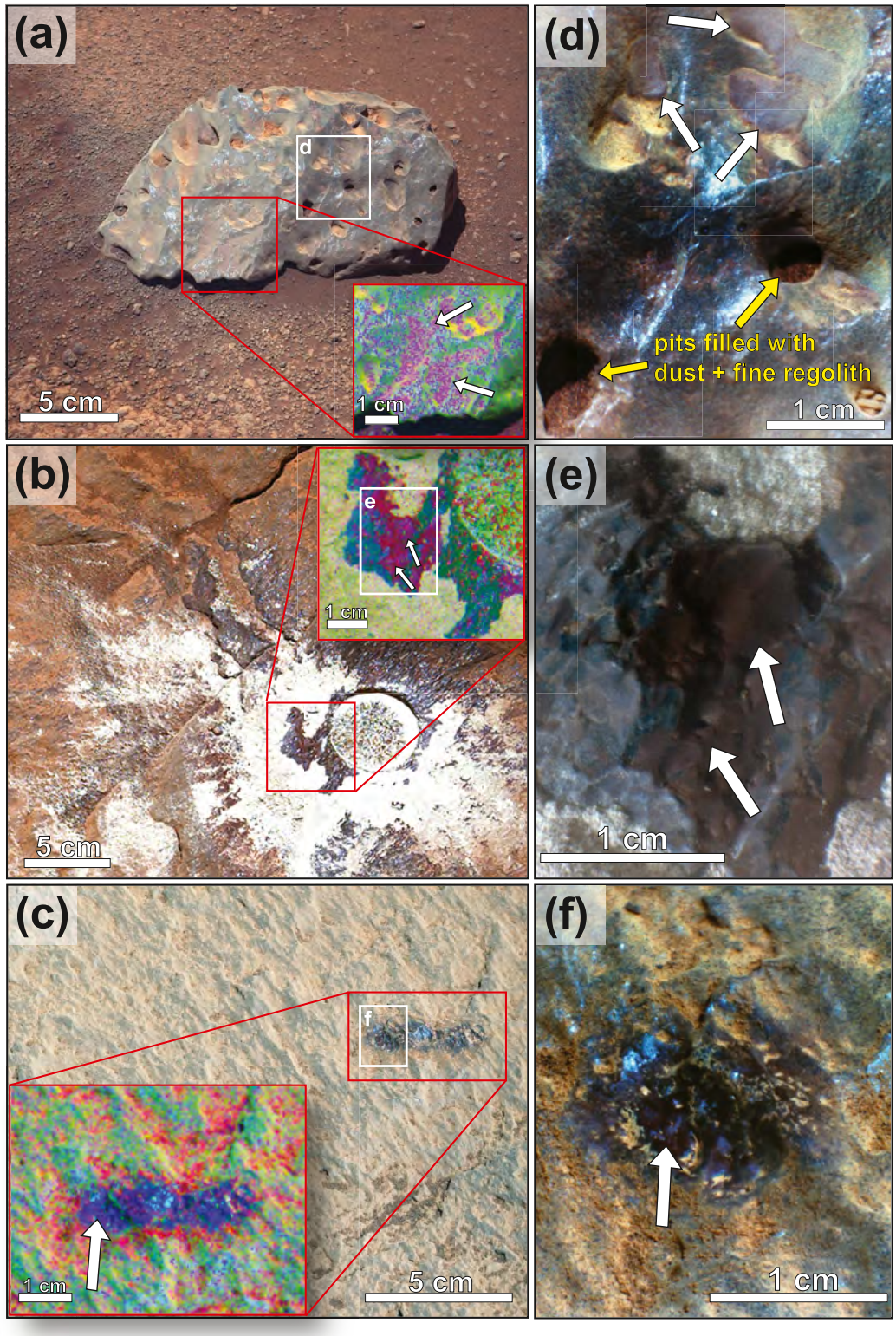

Figure 4.

standard 30 LIBS shots from the SuperCam instrument and revealed presumably the underlying rock (Figure 6d). Some *purple patches* observed on rocks near the Octavia E. Butler landing site occurred near pits/voids filled with fine-grained regolith and dust (Figures 4a and 4d). These features typically exhibited raised surfaces relative to the host rock, possibly a result of differential weathering.

3.1.2. Continuous Coatings

Coatings that were more extensive along rock surfaces (a few 10s of cm across) were typically observed in both the Máaz and Séítah formations on lower lying surfaces near regolith (Figure 7). The color of the coatings were typically more muted or grayer relative to the more purple patches in enhanced color images. In Mastcam-Z L256 DCS composite images, the coatings also exhibited purple hues distinct from the bluer uncoated bedrock; however, in some cases, they were slightly obscured by a thin dust cover (green in DCS images). Occasionally, these coatings were associated with loose, eroded flakes of coatings or coated rock fragments that exhibited smooth and dull surfaces as well as purple hues in Mastcam-Z L256 DCS composite images similar to coatings on nearby rocks (Figure 8). In some places, both *continuous coatings* and *purple patches* occurred on the same rock, where *continuous coatings* occurred near the regolith interface on presumably more recently exposed surfaces and *purple patches* on higher standing, wind abraded, and less dusty surfaces (Figures 7c and 7f). *Continuous coatings* were also occasionally observed along vertical surfaces that may correspond to previously fractured rock, suggesting formation following mechanical weathering of the bedrock (Figures 5a and 5e). Similar to the *purple patches*, the thickness of the *continuous coatings* could not be resolved by the Mastcam-Z PRo3D models and are likely thinner than ∼300 μm.

3.1.3. Thick Coatings

Some localized coatings appeared thicker as they strongly obscured the texture of the underlying rock surfaces. These were only observed along the steep vertical exposures of the Mure outcrop and Artuby ridge within the Máaz formation (Figure 9). Such features typically exhibited a dark gray to purple color in enhanced color images, while the purple hue was most apparent in Mastcam-Z L256 DCS composite images (Figure 10c). These coatings were occasionally observed near thinner *continuous coatings* that were more widespread on rock surfaces (Figure 9d). The thickness and areal extent of these coatings were variable and ranged from small circular raised features (Figure 9f) to thicker and more extensive clumps (e.g., Figure 9g). The latter were typically observed on the sides or undersides of protruding rocks and were not observed on the top of horizontally oriented surfaces. Accurate thickness estimates using Mastcam-Z Pro3D models were possible for select examples shown in Figures 9f and 9g where sufficient stereo coverage and spatial resolution permitted reliable measurements. These coatings were estimated to range from 1 to 20 mm. Some of these coatings appeared to exhibit potential layering with variable thicknesses (Figure 9f), similar to layering observed in some *purple patches*.

3.2. Spectral and Chemical Characteristics

3.2.1. Mastcam-Z Multispectral

Multispectral data indicated that the observed coatings were spectrally - and thus compositionally - distinct from the underlying rock in both the Máaz and Séítah formations. Color differences between coated and uncoated natural rock surfaces were particularly apparent in Mastcam-Z L256 DCS images (Figure 10c). In these images, coatings were distinguished by their purple hues, whereas the uncoated surfaces appeared "bluer." This distinction is further highlighted by the representative ROI spectra shown in Figure 10 as well as the 528 nm band depth versus red/blue ratio spectral parameter values plotted in Figure 11a. Compared to uncoated natural rock surfaces, the coatings (especially the *purple patches*) were typically "redder" with steeper positive slopes between 442 and 754 nm, and stronger 528 nm absorptions consistent with nanophase or crystalline ferric oxides (Figure 3). The spectra of the coatings were also characterized by peak reflectance positions at longer wavelengths

Figure 4. Mastcam-Z (left) and portions of SuperCam enhanced color Remote Micro-Imager (RMI) (right) images showing purple patches class (white arrows) on crater floor rocks. Larger Mastcam-Z context images are Z110 left-eye enhanced color Bayer filter images and white boxes indicate the location of the SuperCam RMI images shown in (d–f). Zoomed insets are DCS L256 composite images highlighting color diversity. (a) Wind abraded surface on Hedgehog (sol 37 zcam03108, Máaz fm.). (b) Post-abrasion, dust-cleared natural surface adjacent to Dourbes abrasion (sol 255 zcam03253, Séítah fm., cleaned by Gas Dust Removal Tool). (c) LIBS-cleared area on Nataani (sol 75 zcam03125, Máaz fm.). (d) Hedgehog (sol 37 scam01037). (e) Cordoeil (sol 268 scam07268). (f) Nataani (sol 75 scam01075).

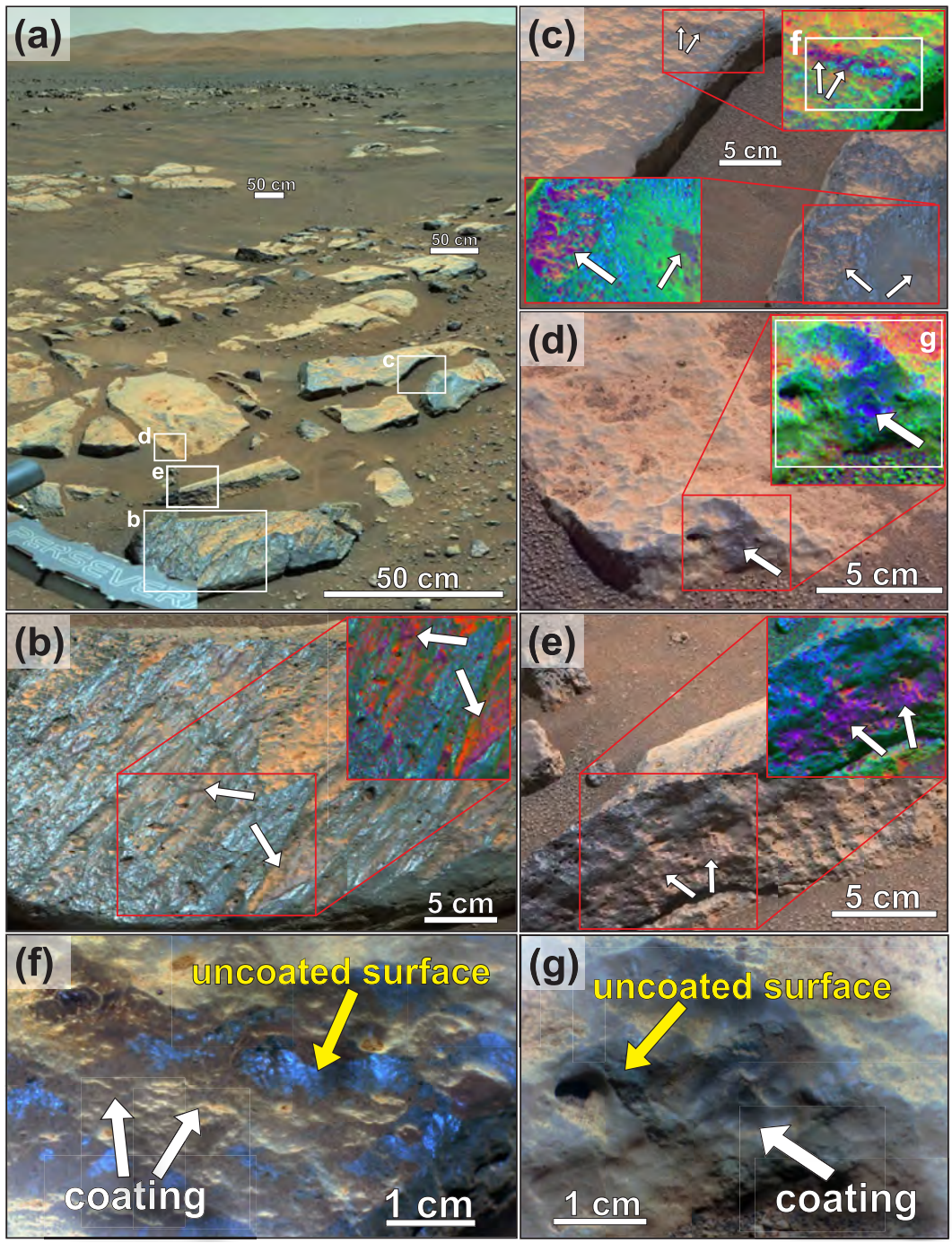

Figure 5. Rock coatings (white arrows) at the Rochette workspace (Máaz fm.). (a) Portion of Rochette workspace mosaic (sol 181, zcam08199) with white boxes showing locations of (b–e). (b–e) Mastcam-Z Z110 left-eye enhanced color Bayer filter images with zoomed insets of DCS L256 composite images highlighting color diversity. White boxes show locations of portions of enhanced color SuperCam Remote Micro-Imager images shown in (f, g). (b) Portion of Estoublon mosaic (sol 182, zcam03210) showing purple patches at Rochette rock prior to abrasion and sampling activities. (c) SuperCam laser-induced breakdown spectroscopy cleared surfaces at Pont (top) and Souche (bottom) (sol 193, zcam03217). (d) Digne les Bains (sol 191, zcam03215). (e) Lance (sol 182, zcam03209). (f) Pont (sol 193, scam01193). (g) Digne les Bains (sol 191, scam02191).

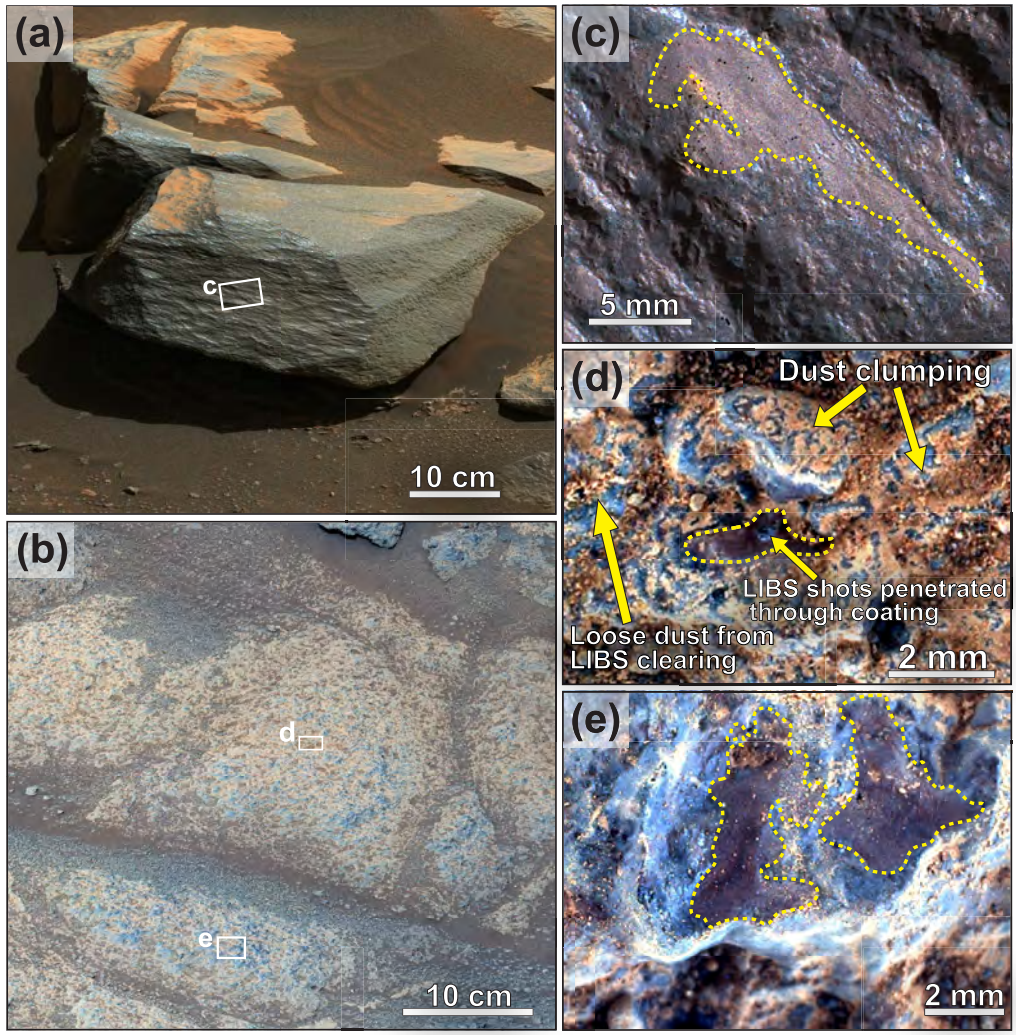

Figure 6. Fine-scale observations of purple patches class (outlined by yellow dashed lines). Portions of Mastcam-Z left eye enhanced color Bayer filter mosaics (left) are shown for context and white boxes indicate locations of enhanced color WATSON images (right). (a) Sid workspace in the Máaz fm. (sol 364, zcam08396, Z34). (b) Foux and Beaujeu workspace in the Máaz fm. (sol 137, zcam08136, Z79). (c) Portion of 7 cm standoff WATSON image showing Alfalfa natural surface pre-abrasion (sol 363, srlc00701). (d) Portion of 6 cm standoff WATSON image showing laser-induced breakdown spectroscopy (LIBS) cleared surface at Beaujeu and nearby dust clumping (sol 141, srlc00448). (e) Portion of 4 cm standoff WATSON image showing LIBS cleared surface at Foux (sol 139, srlc00454).

than those exhibited by the uncoated natural rock surfaces. This spectral distinction was most apparent in the Séítah formation, where the underlying rock was dominated by a peak reflectance position at or below 700 nm and a broad absorption centered near 1,000 nm with a negative slope in the near infrared (NIR), consistent with olivine (Figure 10b, #9).

Despite the differences in lithology and spectral properties between the Máaz and Séítah formations, the coatings were spectrally similar across both crater floor units. For example, *purple patches* identified within Máaz and Séítah both exhibited a similar spectral shape with strong 528 nm absorptions and a broad moderate 910 nm absorption that is consistent with pyroxene or secondary ferric minerals (Figure 10a, #1, 2). However, there were slight spectral differences among the coating morphologies described above. For example, average 528 nm band depth values vary among the morphological classes (Figure 11a). The *purple patch* class generally exhibited the strongest band depths (albeit with some overlap with the *continuous coatings* class) consistent with enhanced oxidation, whereas the *thick coatings* class exhibited the weakest band depths.

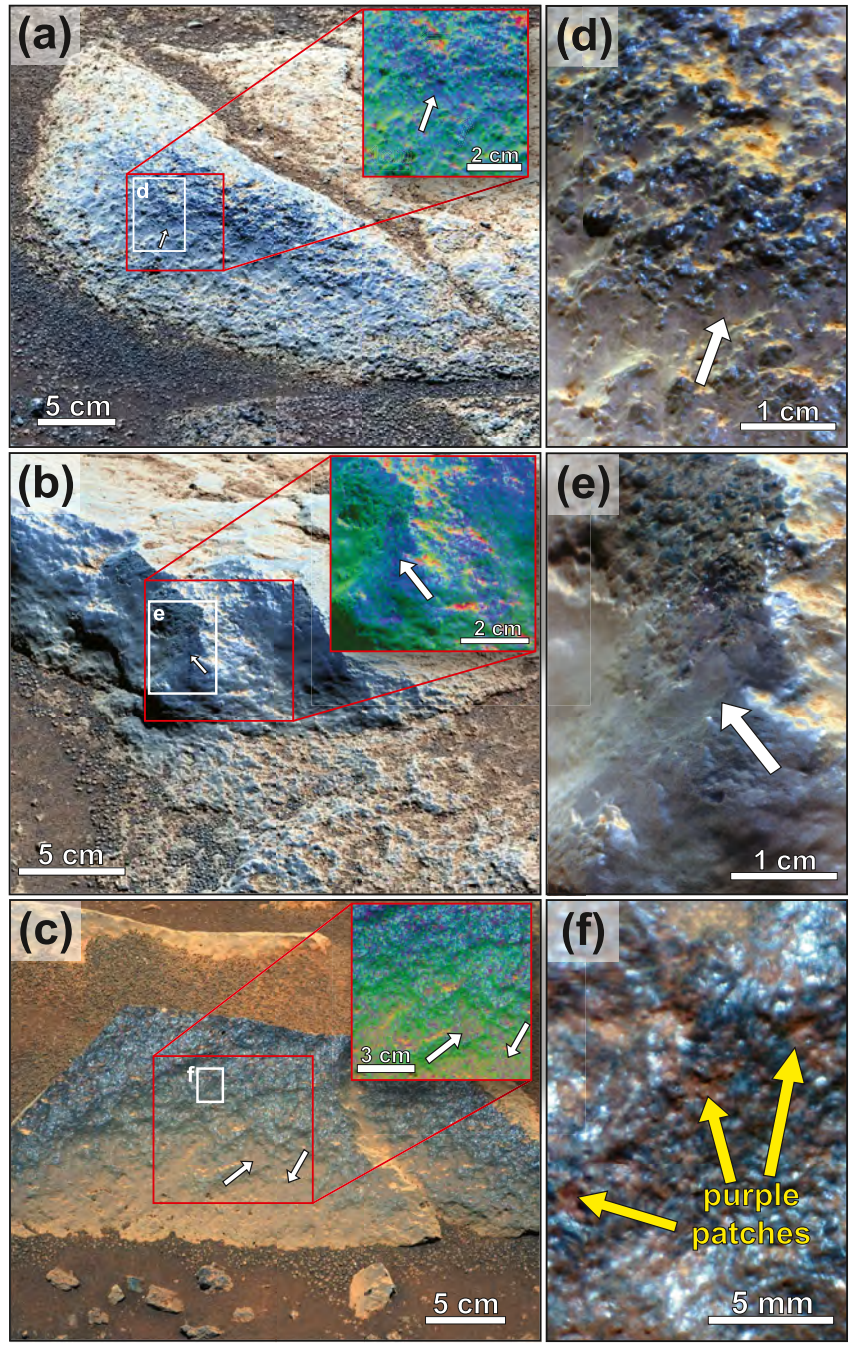

Figure 7. Mastcam-Z (left) and portions of SuperCam Remote Micro-Imager (RMI) (right) images showing continuous coatings class (white arrows) on crater floor rocks. Larger Mastcam-Z context images are Z110 left-eye enhanced color Bayer filter images and white boxes indicate the location of the enhanced color SuperCam RMI. Zoomed insets are DCS L256 composite images highlighting color diversity. (a) Naatsiilid (sol 86, zcam03137, Máaz fm.). (b) Issole (sol 291, zcam03269, Séítah fm.). (c) Tseebii (sol 112, zcam03161, Máaz fm.). (d) Naatsiilid (sol 86, scam05086). (e) Sagnes (sol 291, scam02291). (f) Tseebii (sol 112, scam02112) showing potential purple patches.

The spectral distinction between coating classes was also apparent at longer wavelengths beyond 700 nm in representative spectra shown in Figure 10a. In these spectra, *purple patches* exhibited a broad moderate 910 nm absorption whereas the continuous and *thick coatings* classes lacked a significant 910 nm absorption and occasionally exhibited an overall negative slope between 800 and 1,022 nm as well as a downturn at 1,022 nm

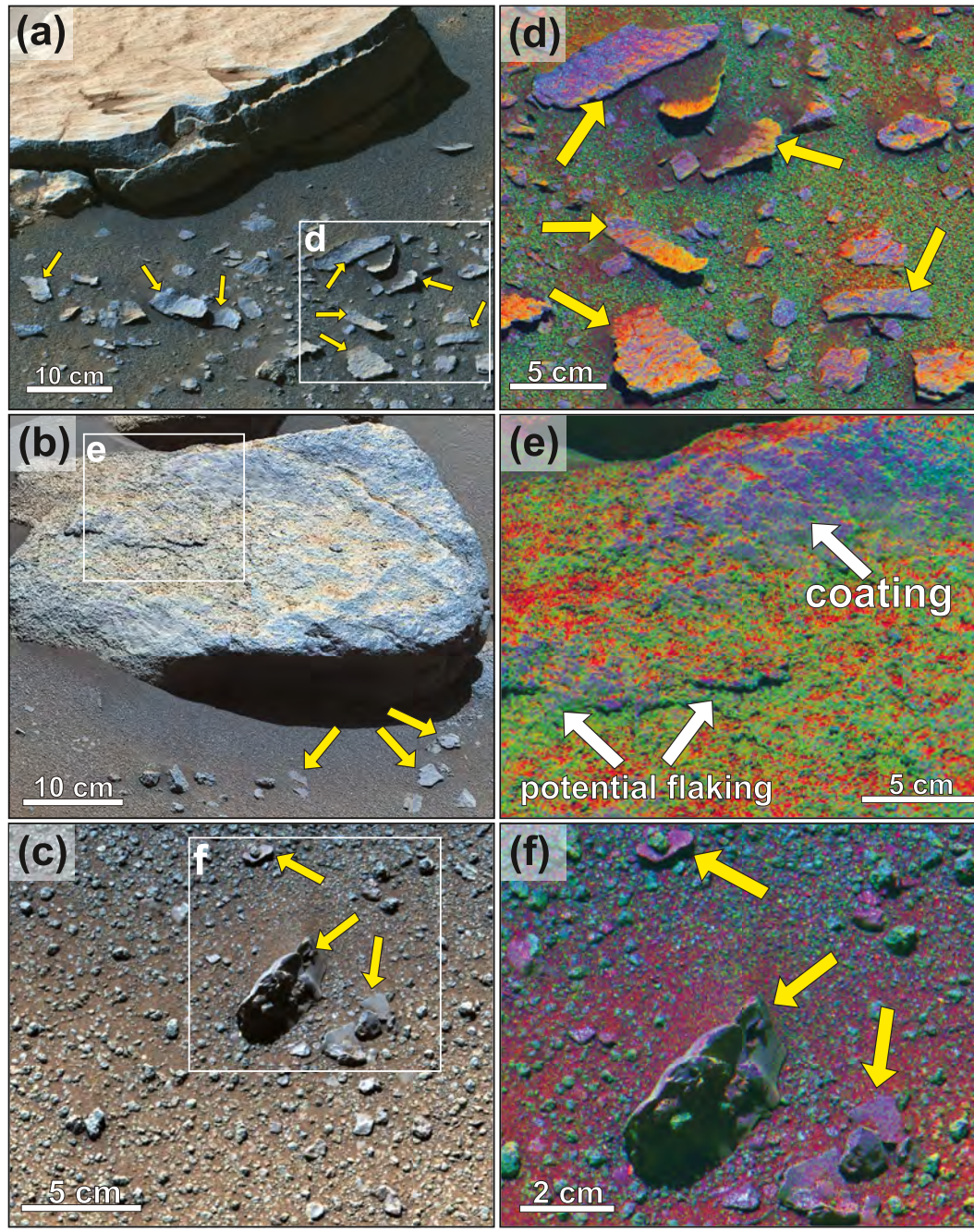

Figure 8. Example of eroded flakes (yellow arrows) associated with the continuous coatings class on the Jezero crater floor. (a–c) Mastcam-Z left eye enhanced color Bayer filter images with white boxes indicating locations of DCS L256 composite images (right) showing purple hues of flakes and nearby coatings. (a) Portion of sol 206 Z110 mosaic (zcam08234, Séítah fm.). (b) Portion of sol 178 Z110 mosaic (zcam08193, Séítah fm.) showing Aiguines rock and nearby flakes. (c) Flakes near the Rimplas workspace in Máaz fm. (sol 346, zcam03315, Z110). (d) Auvere (sol 208, zcam03230, Z110). (e) Aiguines (sol 178, zcam03207, Z110). (f) Les Cluots (sol 346, zcam03315, Z110).

possibly related to hydrated phases (Rice et al., 2010). These differences were less obvious in our spectral parameter analysis of 910 nm band depth versus 800/978 nm ratio in all coating spectra investigated as shown in Figure 11b. While we observed some clustering of points that corresponded to the morphologic class, we also noted more overlap between the classes compared to the visible wavelength spectral parameters shown in

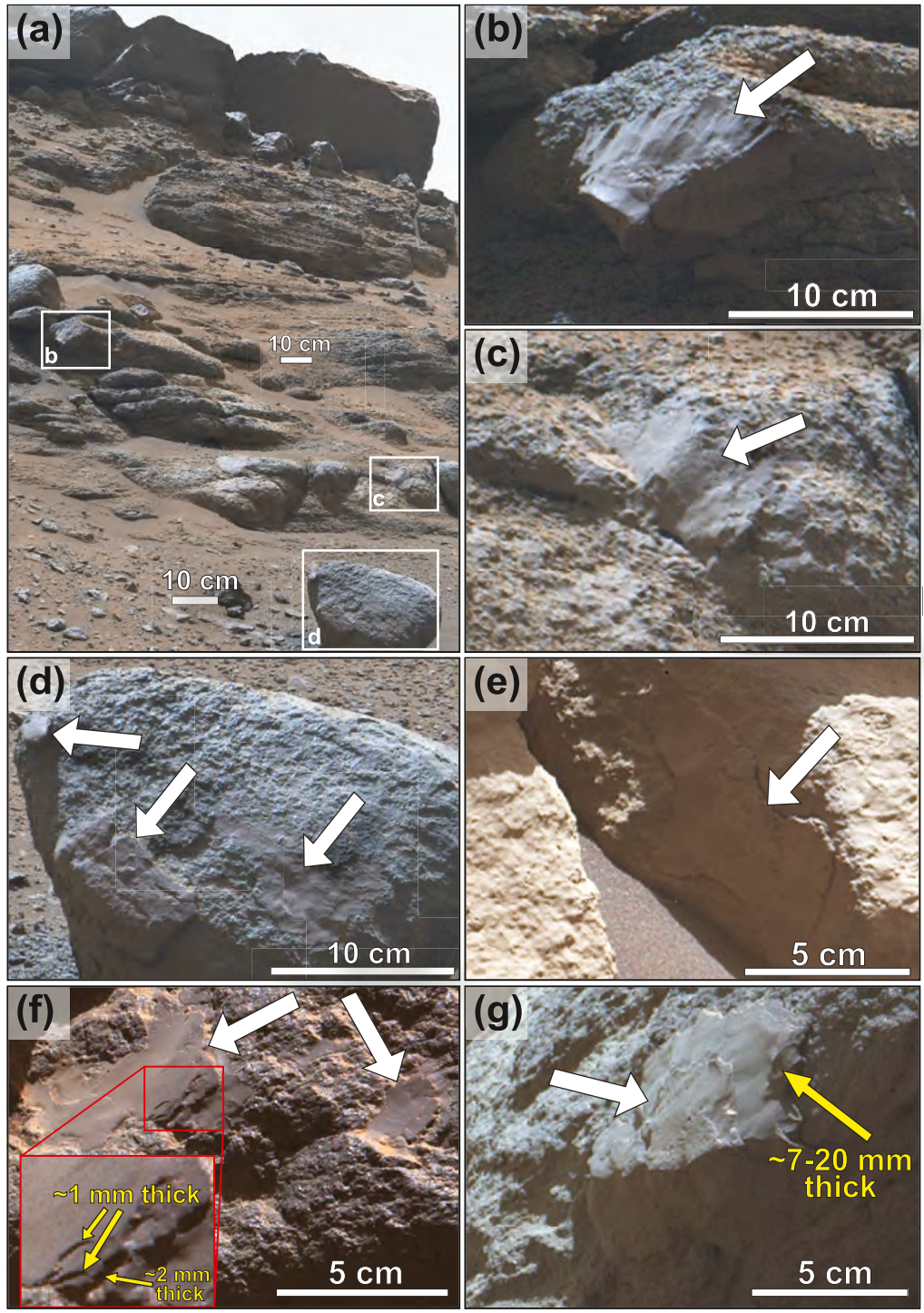

Figure 9. Thicker coatings class examples (white arrows) at Artuby ridge (a–d) and Mure outcrop (e–g). (a) Portion of the Mastcam-Z left eye enhanced color Bayer filter mosaic of Artuby Ridge (sol 342, zcam08367). White boxes indicate locations of zoomed insets in (b–d). (e–g) Portions of Mastcam-Z left eye enhanced color Bayer filter mosaic of Mure (sol 169, zcam08181, Z110) with estimated coating thicknesses derived from PRo3D Software shown in (f) and (g).

Figure 11a. In the 910 nm band depth parameter, the *purple patch* classes exhibited the greatest band depth values while the *thick coatings* class exhibited the smallest values. The classes were less distinct in the 800/978 nm ratio parameter as each class exhibited a similar range of values.

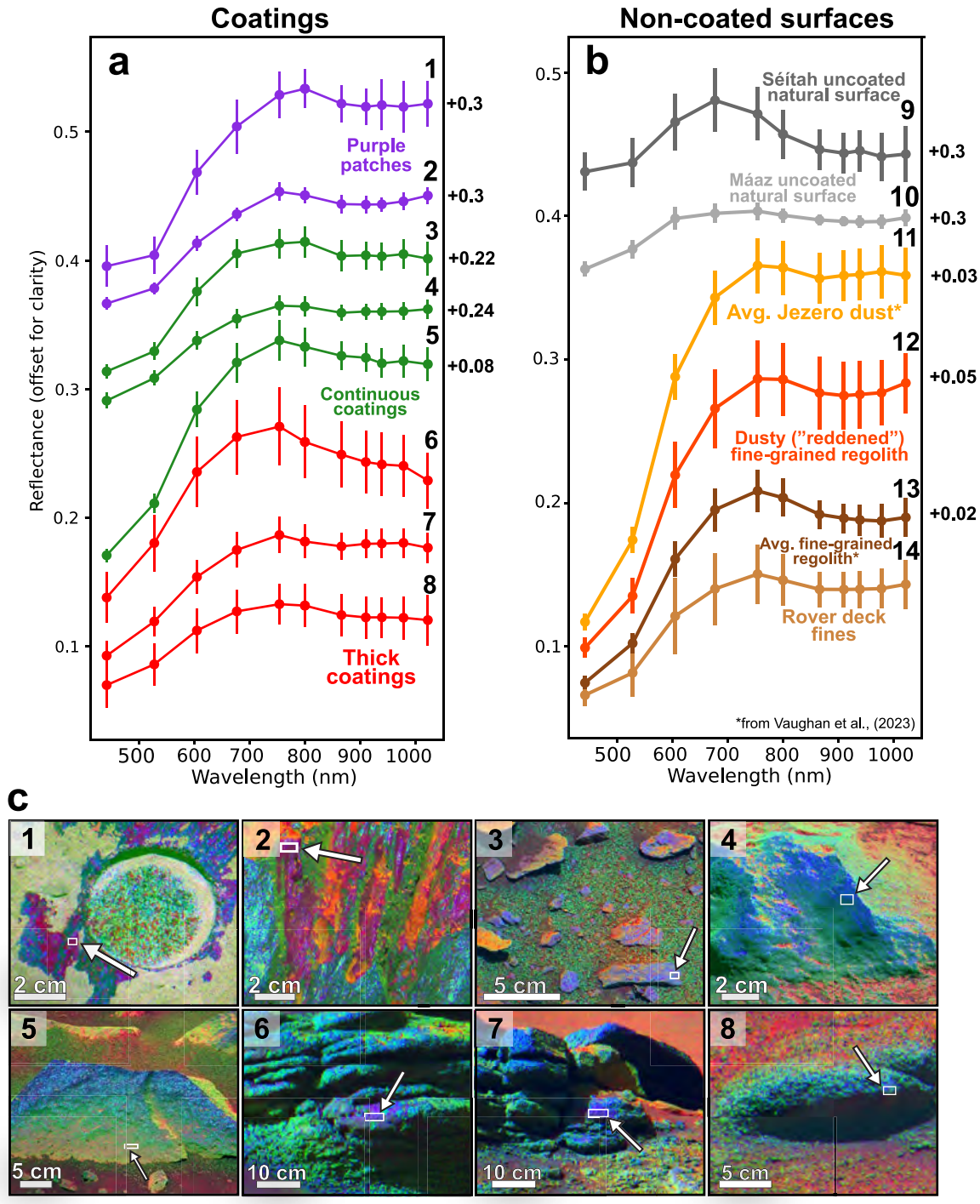

Figure 10. Mastcam-Z multispectral data of rock coatings and non-coated surfaces including regolith and dust. Spectra are stacked for clarity and amounts of offset are noted. Spectra shown here are from the multispectral database available in Rice et al. (2022). (a) Representative spectra from the purple patches class (purple), continuous coatings class (green), and thick coatings class (red). Names of coated targets represented here are specified in the archived table available in Garczynski (2025). (b) Representative spectra from uncoated surfaces, including Séítah natural surface (Dourbes, sol 255, zcam03253), Máaz natural surface (Manior, sol 188, zcam03214), dusty fine-grained regolith (Naadin, sol 92, zcam03143), and rover deck fines (rover deck, sol 344, zcam03312). Average dust and fine-grained regolith are from Vaughan et al. (2023). (c) L256 DCS composite images with white outlines indicating regions of interest for spectra shown in (a).

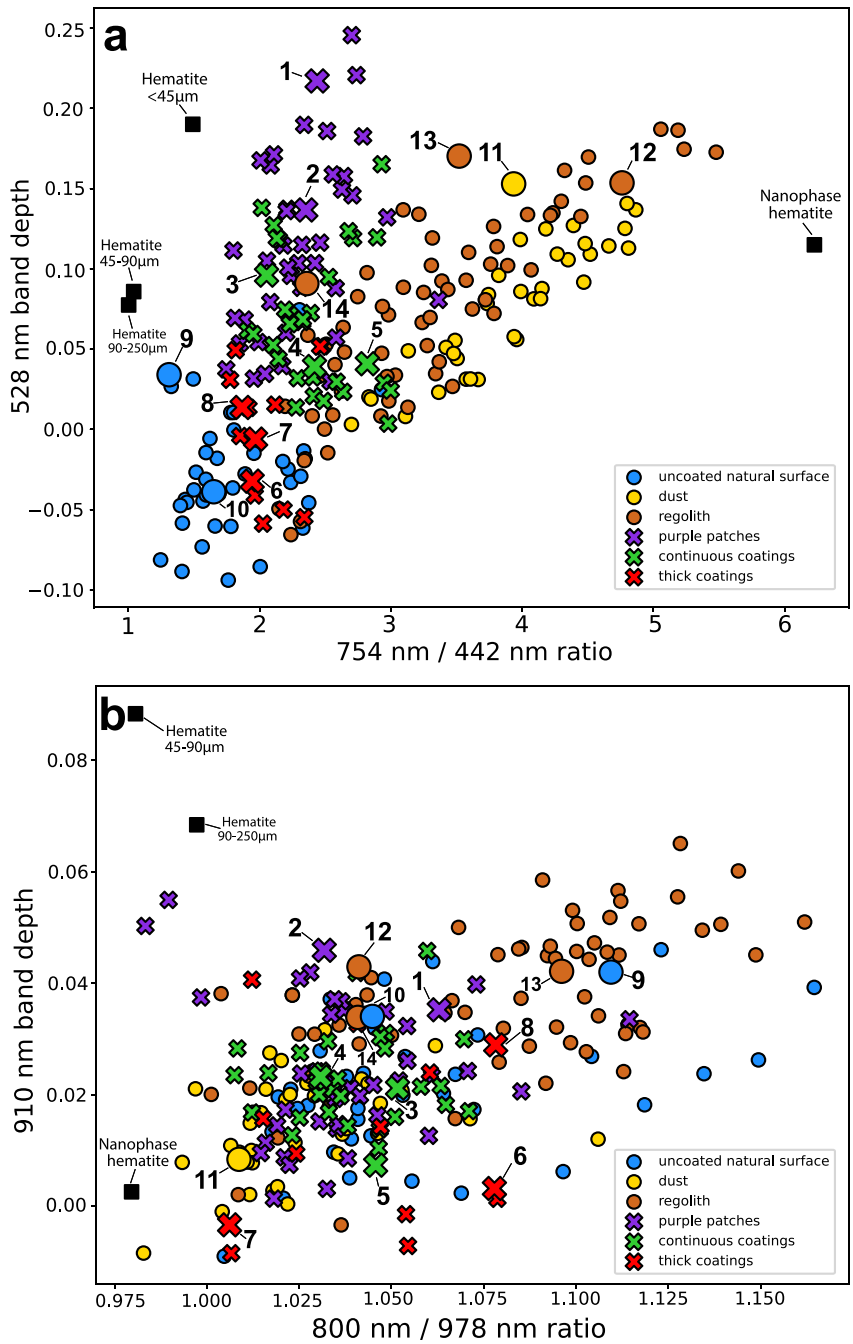

Figure 11. Mastcam-Z spectral parameter plots of (a) red/blue (754 nm/442 nm) ratio versus 528 nm band depth and (b) 800 nm/978 nm ratio versus 910 nm band depth. Cross symbols represent coatings and are colorized by coating morphology including purple patches (purple), continuous coatings (green), and thick coatings (red). Circle symbols represent non-coated surfaces including natural rock surfaces (blue), dust (yellow), and regolith (orange). Enlarged and numbered points correspond to numbered spectra plotted in Figure 10. Black squares indicate spectral parameters of various hematite laboratory references. Regions of interest spectra used in parameter analysis are available in a multispectral database from Rice et al. (2022) and Mastcam-Z observations analyzed here are specified in the archived table available in Garczynski (2025).

It is important to note that our multispectral coverage (particularly nearfield) of the thicker coatings is limited and were typically acquired at earlier times of day (before 9:15 local true solar time (LTST)) and high incidence angles (≥40°) due to illumination constraints on the steep northern facing exposure of the Artuby ridge. Nearly all

other multispectral observations were acquired close to local noon (between 10:30 and 13:30 LTST) when assumptions in the calibration pipeline were most accurate (Rice et al., 2023). It is possible that the weakened 528 nm absorptions and negative NIR slopes present in the *thick coatings* spectra were related to calibration issues resulting from the earlier acquisition times and high incidence angles, but further investigation will be needed to constrain the effects.

A comparison between the various coatings and the local regolith and dust revealed some spectral similarities but notable differences. While all coatings spectra exhibited a similar range of 528 nm band depths compared to those of regolith and dust, the greatest band depth values were observed in some of the *purple patch* class spectra. Additionally, spectra of regolith and dust were typically redder as the coatings spectra generally plotted separately with smaller red/blue ratio values suggesting compositional differences and potentially consistent with a mixture of crystalline hematite and/or other crystalline ferric phases (Figure 11a). At wavelengths beyond 700 nm, spectra of both *purple patch* coatings and regolith exhibited some of the greatest 910 nm band depths although the latter generally showed much greater 800/978 nm ratio values attributed to coarser olivine-bearing sand derived from the erosion of Séítah bedrock (Figure 11b; Vaughan et al., 2023). The *purple patch* coating spectra with the strongest 910 nm band depths were more similar to the finer-grained regolith likely composed of a mixture of pyroxene and ferric materials (Figure 10; Vaughan et al., 2023). These coating spectra were particularly similar to that of dark fine-grained regolith that was deposited on the *Perseverance* rover deck by strong winds during a regional dust storm, possibly suggesting a similar composition (Figures 10b and 11 #14; Lemmon et al., 2022; Vaughan et al., 2023). The rover deck grains likely represented some of the finest fraction of regolith larger than airfall dust that was uncontaminated by the coarser olivine-bearing regolith as evident by the lack of a negative slope between 800 and 1,022 nm in the spectrum compared to that of average Jezero fine-grained regolith from Vaughan et al. (2023) (Figures 11b and 12 #13). A spectrum of dusty ("reddened") fine-grained regolith also exhibited a broad 910 nm absorption similar to some of the *purple patch* class coatings and rover deck fines, but had a much stronger red slope in the visible range likely related to higher dust content (Figures 11b and 12 #12). Spectra of thick dust generally lacked a significant broad 910 nm absorption and were characterized by a relatively neutral slope between 800 and 1,022 nm consistent with the presence of nanophase hematite (Figure 3). Despite the coating spectra being overall "bluer" compared to dust spectra as shown in Figure 11a, some of them exhibited similar spectral characteristics beyond 700 nm. In particular, the spectra of the *continuous coatings* class generally lacked significant 910 nm absorptions and had a similar neutral slope suggesting a potential compositional relationship with dust. It is also possible that the similar characteristics in these coating spectra were due to spectral contamination by dust as many of the *continuous coatings* were located on lower lying dusty rock surfaces.

As summarized in Table 3, our Mastcam-Z spectral analysis suggested that the coatings were compositionally distinct from the underlying rock and likely composed of externally sourced material. Spectral variability both within and across coatings classes suggested a varying mixture of ferric materials, with the *purple patches* class consistent with the most oxidized of the coatings. While coatings spectra were significantly "bluer" than spectra of dust and regolith suggesting some compositional differences, we cannot rule out potential contributions from fine-grained regolith and dust to the formation of the coatings due to some similar characteristics at the longer wavelengths.

3.2.2. SuperCam VISIR

Relative reflectance spectra from the SuperCam VISIR instrument helped further characterize the spectral properties of the coatings and their relationship with underlying bedrock, dust, and fine-grained regolith. Figure 12 shows average SuperCam VISIR spectra of *purple patches*, *continuous coatings*, Máaz and Séítah abraded surfaces as well as dust and fine-grained regolith. Data of thicker coatings observed along the Artuby ridge and Mure were not included as the *Perseverance* rover did not acquire any SuperCam VISIR data on these features during its traverse. As reported by Mandon et al. (2023), the coatings exhibited red slopes at shorter wavelengths (~0.6–0.8 μm), greater 0.545 μm band depths, relatively flat to blue-sloped spectral shapes beyond 1.3 μm, weak 1.9 μm water absorptions possibly related to hydrated mineral phases or adsorbed water, and a slight negative slope beyond ~2.35 μm possibly consistent with sulfates. The red slopes and absorptions in the visible wavelengths were consistent with Mastcam-Z multispectral data, and further support a component of ferric oxides. While the average spectrum of the *purple patch* class coatings appeared similar to that of the *continuous coatings* in Figure 12a, a spectral parameter analysis of 0.545 μm band depth versus 1.93 μm band depth revealed

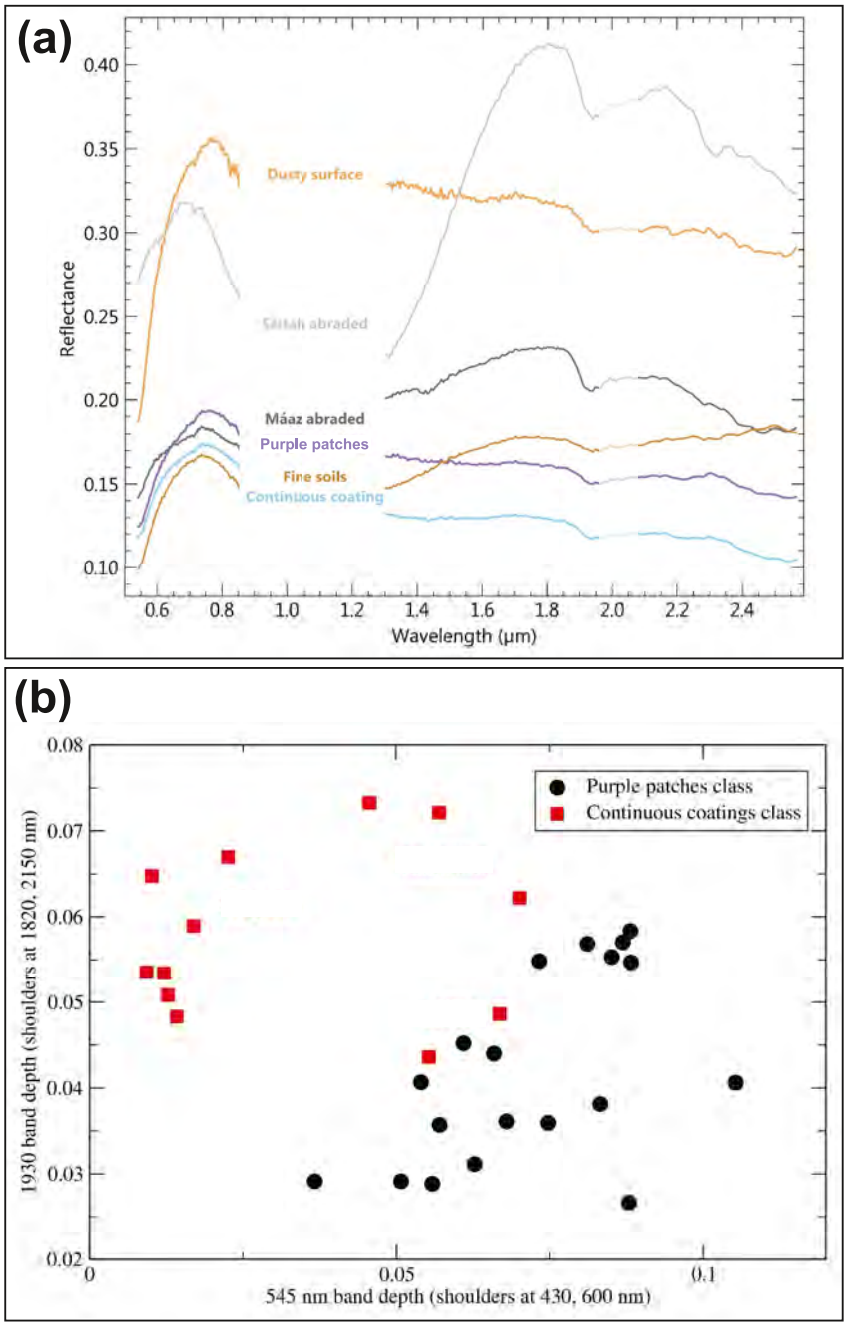

Figure 12. SuperCam visible and short-wave infrared reflectance (VISIR) observations of crater floor coatings. (a) Average SuperCam VISIR spectra of coatings, abraded surfaces, dust, and fine-grained regolith. Spectra of dust, abraded surfaces, and fine soil are from Mandon et al. (2023). Purple patches spectrum represents an average of 17 individual point spectra from four different coating targets. The continuous coating spectrum represents an average of 12 individual point spectra from three different coating targets (Figure S1 in Supporting Information S1, Garczynski, 2025). Segments of the spectra shown in lighter color near 2 μm correspond to the main atmospheric CO_2 absorption region, where residuals might affect the spectra. (b) Spectral parameter plot showing band depths of purple patches and continuous coatings class point spectra analyzed in (a) at 545 nm (sensitive to crystalline ferric materials) and 1,930 nm (sensitive to hydration).

some notable differences between the two morphologic classes as shown in Figure 12b. Here we observed that the spectra of coatings from the *purple patch* class had greater 0.545 μm band depths than the *continuous coatings* spectra, which was consistent with the Mastcam-Z results and further suggested that the *purple patch* coatings were more oxidized. An opposite relationship was observed in the 1.93 μm band depth parameter as spectra of

Table 3
Summary of Coating Spectral and Chemical Results

Mastcam-Z multispectral (Figures 10 and 11)	SuperCam VISIR (Figure 12)	SuperCam LIBS (Figures 13 and 14)
Consitent with presence of crystalline hematite and/or other crystalline ferric phases; spectrally distinct from bedrock	Consistent with presence of crystalline ferric phases and sulfates; spectrally distinct from berock	Chemically similar to mean dust and disturbed soil with relative enrichment in Ca; presence of hydrated Mg/Ca sulfates as reported by Meslin et al. (2022)
Purple patches are most oxidized followed by *continuous* and *thick coatings*	Overall weakly hydrated and similar spectral shape to dust at longer wavelengths	Composition distinct from bedrock; no significant chemical variability observed in coatings across formation or morphologic class
	Purple patches are more oxidized but less hydrated than *continuous coatings*	

continuous coatings exhibited greater values suggesting more hydration compared to the coatings of the *purple patch* class.

The SuperCam VISIR data were also consistent with the Mastcam-Z results in suggesting that the coatings were compositionally and mineralogically distinct from the underlying bedrock, further supporting an external origin. Average spectra of Máaz and Séítah abraded surfaces exhibited spectral shapes that were distinct from those of the coatings. While both the underlying rock and coatings exhibited water absorptions near 1.9 μm, those associated with the coatings were much weaker and may suggest that they were overall less hydrated than the bedrock (Figure 12a).

A VISIR spectral comparison of the coatings and dust indicated that the two were spectrally and compositionally similar, suggesting the latter may play an important role in coating formation. Despite the dust spectrum exhibiting stronger red slopes in the ∼0.6–0.8 μm range and higher overall reflectance across the SuperCam wavelength range, both coatings and dust shared a similar overall spectral shape beyond ∼1.3 μm, including a faint 1.9 μm water absorption and a slight downturn beyond ∼2.35 μm possibly consistent with sulfates (Figure 12a). The stronger ∼0.9 μm absorptions observed by Mastcam-Z in some of the *purple patch* class coating spectra compared to dust spectra were unable to be investigated in the VISIR data as these features fall outside the spectral range of SuperCam.

Fine-grained regolith and coatings appeared spectrally distinct in the VISIR range as viewed by SuperCam. While coatings and fine-grained regolith exhibited similar red slopes in the visible range and a relatively weak 1.9 μm water absorption, fine regolith exhibited two broad absorptions in the ∼0.7–1.7 and ∼1.7–2.4 μm ranges consistent with pyroxene possibly mixed with olivine (Mandon et al., 2023), and no downturn beyond ∼2.35 μm. The second absorption centered around 2 μm suggested low-Ca pyroxene and was consistent with the ∼0.9 μm absorptions observed in Mastcam-Z spectra of fine-grained regolith. Mixing of pyroxene with oxides could decrease the depth of the larger bands leaving behind only the stronger ∼0.9 μm absorptions. While it is unclear whether the contribution of fine-grained regolith is causing the ∼0.9 μm absorptions observed in some of the Mastcam-Z coating spectra, it is possible that additional oxides in the coatings can explain the weaker broad absorptions in the VISIR spectra of coatings.

3.2.3. SuperCam LIBS

Elemental abundances from SuperCam LIBS were used to investigate the chemical composition of coatings and their potential relationship with bedrock, fine-grained regolith, and dust. Figure 13 shows molar compositions derived from MOC plotted in Si + Al/Fe + Mg/Na + Ca + K and Ca/Mg/Fe ternary diagrams. Despite the obvious chemical differences between the Mg-rich Séítah rocks and the relatively Mg-poor Máaz rocks, the surface coatings were overall chemically similar regardless of their location on the crater floor (Figures 13a and 13b). This is consistent with the spectral data from SuperCam VISIR and Mastcam-Z, further showing that there is no direct compositional relationship between the coatings and the underlying rock.

Overall, we did not observe any major differences between the morphologic classes of coatings suggesting a similar chemical composition (Figures 13c and 13d). Despite the clumping of most coating data points, we observed a few points within the *purple patch* and *continuous coatings* class that trended away towards chemical endmembers including Si + Al and Fe + Mg (Figures 13a and 13c) and Mg (Figures 13b and 13d). Visual

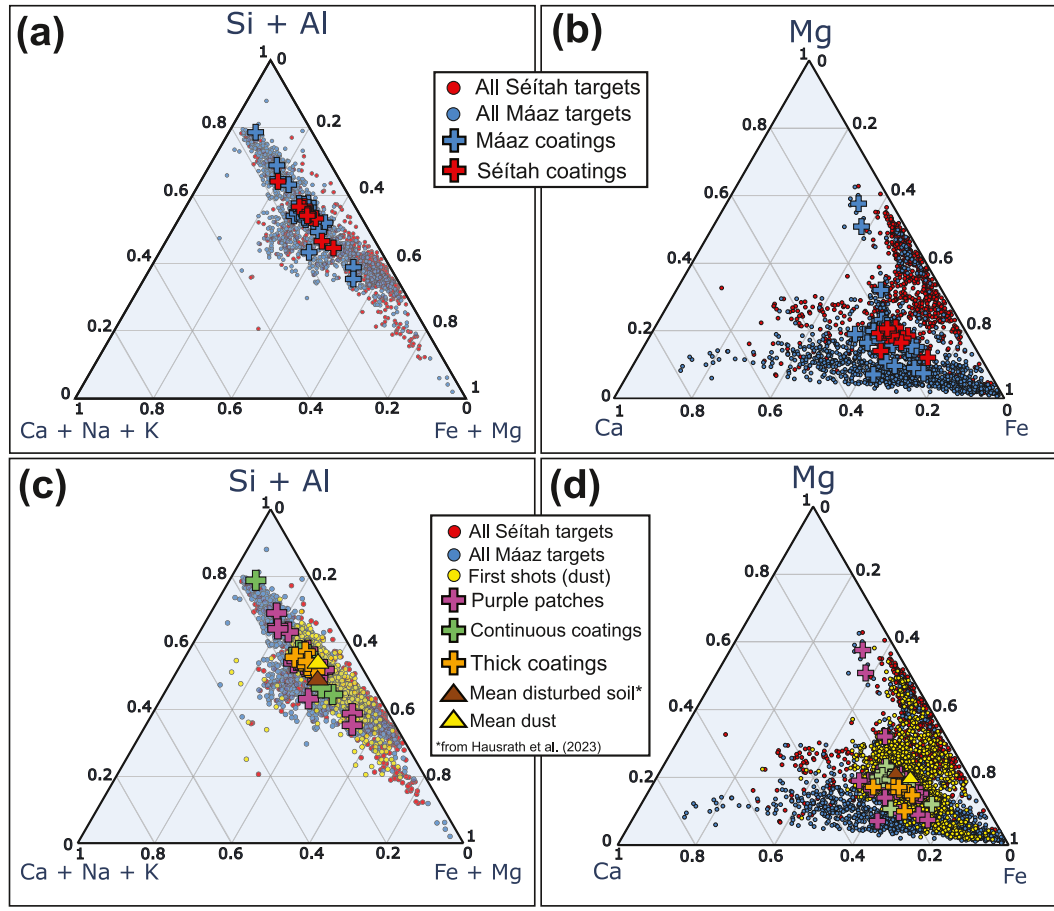

Figure 13. SuperCam laser-induced breakdown spectroscopy (LIBS) observations showing elemental compositions of coatings, underlying bedrock, fine-grained regolith, and dust. Coating points are colorized by crater floor unit (a, b) and coating morphology (c, d). Analyzed LIBS points of coated targets are shown in Figure S1 in Supporting Information S1 and coating type is specified in the archived table available in Garczynski (2025). (a) (Si + Al), (Fe + Mg), (Na + Ca + K) ternary diagram showing Máaz and Séítah coatings compared to underlying bedrock. (b) Ca-Mg-Fe ternary diagram showing Máaz and Séítah coatings compared to underlying bedrock. (c) (Si + Al), (Fe + Mg), (Na + Ca + K) ternary diagram showing various coating morphologies compared to underlying bedrock, dust, and fine-grained regolith. (d) Ca-Mg-Fe ternary diagram showing various coating morphologies compared to underlying bedrock, dust, and fine-grained regolith.

examination and comparison to bedrock targets confirmed that these points were not due to contamination from underlying bedrock but instead corresponded to local variability in the coating.

Dust and fine-grained regolith were chemically similar to the coatings, suggesting a potential compositional relationship. However, coatings appeared to be enriched in Ca relative to the dust and fine-grained regolith (Figure 13d). This enrichment suggests an additional component in the coatings and is likely consistent with Ca-sulfate as reported by Meslin et al. (2022). While this study did not focus on minor and trace element abundances derived from the LIBS data, we did note that a preliminary assessment revealed that the coatings were not enriched in Mn relative to the underlying bedrock as observed in terrestrial rock varnish.

In some specific cases, SuperCam investigated purple coatings with a depth profile of 125 shots to look for any chemical variability with depth. For instance, target Chokecherry (Sol 378, Máaz fm.) was analyzed with three points that hit the coating and the last point that sampled the bedrock (Figure 14a). The shot-to-shot evolutions of MgO, Al_2O_3, FeOT, and Na_2O (Figure 14b) show that the first ~40 shots on the coating (point #2) are chemically different from the last part of the burst, with higher MgO, Al_2O_3, and Na2O and lower FeO_T. On the other hand, the composition reached after the ~40th shot is comparable with the composition of the bedrock at point #4, which is more homogeneous along the burst. This confirms that the *purple patch* is a surface layer chemically different from its host rock, and suggests that the laser penetrated through this coating. The fact that the transition

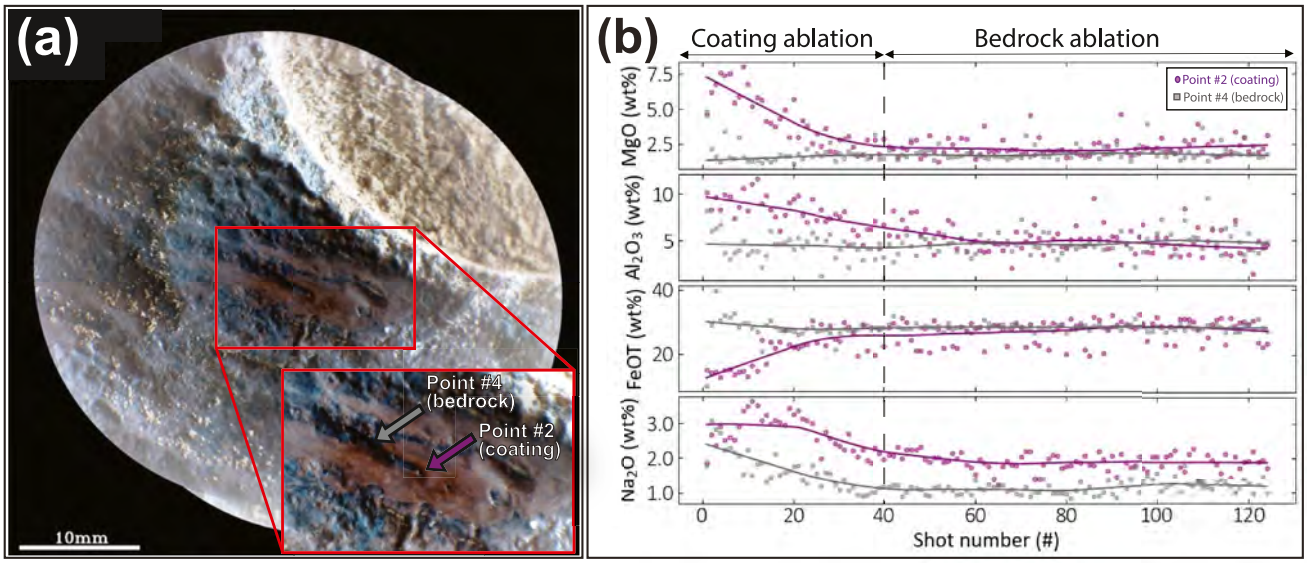

Figure 14. SuperCam depth profile on Chokecherry in the Máaz fm. (sol 378, scam01378). (a) Remote Micro-Imager context image (Gaussian stretch) of the observation showing the four laser footprints, three hit the coating and one hit the bedrock for reference. (b) Comparison of the shot-to-shot evolution of the Major Oxide Composition for MgO, Al_2O_3, FeOT, and Na_2O for point #2 on the coating and point #4 on the bedrock.

from the coating to the host rock is smooth is because the laser keeps ablating the coating on the walls of the crater, even after reaching the host rock at the bottom of the laser pit (Lanza et al., 2015). This data set suggests that the thickness of the coating probed on point #2 was between 60 and 150 μm (Chide et al., 2021; Wiens et al., 2021). However, this thickness is very variable between the points and a more in-depth analysis of these depth profiles is required for future studies.

4. Discussion

Rock coatings were commonly observed on the Jezero crater floor and these features likely represent a unique episode of alteration that may have been more recent in the crater's history. The widespread nature of the coatings in both the Máaz and Séítah formations suggests that this activity may have affected the entire crater floor following the emplacement and subsequent erosion of the crater floor units. Spectral signatures consistent with ferric oxides, sulfates, and hydrated phases suggest the important role of water in the formation of these coatings. Our results show that these surface features are likely compositionally distinct from the underlying bedrock and are composed of a mixture of externally derived sediment providing further evidence that these features are coatings rather than a weathering rind. The high frequency of these coatings observed at both the outcrop and microscale highlights the importance of characterizing these features as these coatings in many cases may have obscured the underlying rock or contaminated our natural surface observations aimed at interpreting bedrock lithology. In the following sections, we explore in more detail the potential formation mechanisms of these coatings, their timing, and the implications for understanding the larger alteration history of not only Jezero crater but also Mars.

4.1. Potential Formation Mechanisms

Previously proposed models for coating formation on Mars involve both physical interactions of windblown fine dust/soil particles as well as the chemical interaction of reactive sulfate salts and/or ferric phases (including iron oxyhydroxide species) with water (Bishop et al., 2002). Other hypotheses for the coatings included anhydrous formation mechanisms such as the deposition of volcanic vapors (Schmidt et al., 2024). The hydrous models suggest that original 1–3 μm dust/soil particles, containing fine-grained silicate particles mixed via aeolian processes with reactive sulfate or ferric oxyhydroxide phases, are initially deposited on rock surfaces as loose dust cover. Electrostatic charges can coalesce these dry fine grains, which may aggregate into larger particles and become further stabilized at the surface (Bridges & Muhs, 2012). Water interaction with the reactive components can bind the chemically neutral silicate particles, forming a hardened coating that can only be removed by

subsequent sand abrasion. Similar mechanisms can occur within drift deposits to form cemented soils or duricrusts (Bishop et al., 2002), which previous studies have suggested to be globally distributed on the Martian surface (Jakosky & Christensen, 1986). In these models, the water needed for coating formation may come from diurnal moisture variations, frost, meltwater, or other near surface aqueous activity (Bishop et al., 2002).

Our investigations of coatings on the Jezero crater floor revealed that the observed surface features may be consistent with previously proposed models of coating formation and suggest a similar formation mechanism. The coatings observed at Jezero are likely composed of a mixture of sediment indurated and cemented to the rock surface. The spectral and chemical similarities observed in the SuperCam IR and LIBS data between coatings and dust strongly suggest a potential genetic link and that bright airfall dust may play an important role in coating formation. Observations of dust clumping, likely due to electrostatic forces, in close proximity to coatings are consistent with previously proposed models as this process may be an important precursor to coating formation at Jezero (Figure 6d).

However, an additional component may be present, as evidenced by (a) the weaker red slopes observed in the visible range of both SuperCam and Mastcam-Z coating spectra compared to dust spectra; (b) the presence of a broad 910 nm absorption seen in Mastcam-Z spectra of some *purple patch* coatings and its absence in dust spectra (Figure 10). These differences may be due to the presence of more crystalline phases such as hematite or other ferric-bearing material. It is possible that the 910 nm absorption observed in some of the Mastcam-Z coating spectra was caused by contributions from the pyroxene- and ferric iron-bearing fine-grained regolith, which exhibited similar spectral absorption features. This may be further supported by the chemical similarities we observed in the LIBS data between fine-grained regolith and the coatings (Figure 13). As we noted earlier, while the fine-grained regolith appeared spectrally distinct from the coatings in the SuperCam VISIR data, it is possible that additional oxides in the coatings may explain the weaker broad absorptions observed in the coating spectra. While previously proposed models suggest the indurated coating material has grain sizes of 1–3 μm, we cannot rule out a component of the darker-toned and potentially locally derived silt-sized regolith (~4–21 μm grain size) in the coatings, but further investigation is needed to constrain any compositional relationship.

The presence of hydrated signatures observed in the SuperCam VISIR data provides additional evidence for previous water interaction. It is possible that some of these hydrated phases were inherited from the hydrated phases present in Martian dust/regolith (Lasue et al., 2022) or formed during subsequent water interaction related to diurnal moisture variations, frost, meltwater, and/or other aqueous events. Meslin et al. (2022) reported the presence of hydrated sulfates in crater floor coatings, some of which may be associated with contribution from dust. The chemical enrichment in Ca of coatings relative to dust and fine-grained regolith, likely associated with Ca-sulfate, suggests the presence of additional salts that were incorporated during coating formation. Mg enrichment observed in some of the SuperCam LIBS data of coatings suggests the presence of Mg-sulfates and is consistent with previously reported results in Meslin et al. (2022). Hausrath et al. (2023) reported similar compositions in an indurated "dust crust" observed on a crater floor rock that is likely consistent with the surface coatings described in this study. PIXL results of the "crust" showed enrichment in SO_3 and Cl relative to airfall dust likely related to a salt cement, and strong correlations between Mg and SO_3 suggested the presence of Mg-sulfates. PCA using shot-to-shot SuperCam data showed tight correlation between Mg and H, suggesting the Mg-sulfates were hydrated.

Soil crusts observed in disturbed regolith throughout the Jezero crater floor (Hausrath et al., 2023) may have formed under similar aqueous conditions as suggested by previously proposed models (Bishop et al., 2002). Analysis of soil crusts indicated the presence of hydrated Mg/Ca sulfates, hypothesized to have formed as a result of atmospheric deposition of Cl- and S-bearing aerosols that were then hydrated with changes in relative humidity and potential frost events (Hausrath et al., 2023; Vakkada Ramachandran et al., 2021). Following the deliquescence of these salts, rapid evaporation during the day may have caused the wicking of brines towards the surface and eventually the efflorescent growth of salts that cemented the soil forming a crust. Subsequent reworking and transport of these crusts by aeolian processes may have contributed to the formation of younger crusts (Hausrath et al., 2023). It is likely that the processes involved in soil crust formation were similar to those that helped indurate and cement the rock coatings, but further investigation is needed to constrain the relationship between the two surface features.

The observations of *continuous coatings* on lower-lying or recently exposed rock surfaces near regolith suggest the important role of burial in coating formation and/or preservation (Figure 7). Regolith cover may have

provided suitable alteration conditions by allowing thin films of water to persist and also protected the newly formed coatings from wind abrasion (Knoll et al., 2008). Furthermore, coatings observed near pits/voids and along potential rock fractures suggest these features may have provided accumulation zones for dust and fine-grained regolith prior to burial and subsequent induration by subsurface fluids. While the extent to which fine-grained regolith is incorporated into the coatings is unclear, our results suggest that shallow burial by regolith may be a key step in coating formation.

The three endmember morphological types of coatings may represent different erosional expressions and maturity of coatings that share a similar origin. This is supported by observations of *purple patches*, *continuous coatings*, and *thick coatings* sometimes occurring in close proximity (Figure 15) and occasionally on the same rock surface, as well as the chemical similarities between the coatings classes we observed in the SuperCam LIBS data. On some rocks investigated by the *Perseverance* rover, we observed more extensive *continuous coatings* occurring on lower-lying surfaces that may have recently been exhumed. These *continuous coatings* were not present on the higher standing wind abraded surfaces that have likely experienced longer periods of aeolian erosion. Rather, these higher standing surfaces exhibited discontinuous *purple patches* on a finer scale, suggesting that the *purple patches* may be eroded, polished, and less dusty expressions of the more *continuous coatings* (Figures 7c and 7f). This may explain our observations of *purple patch* coatings exhibiting the strongest ferric signatures in both the SuperCam VISIR and Mastcam-Z data as the longer surface exposure may have resulted in the *purple patch* coatings being more oxidized possibly enhanced by interaction with highly oxidative photochemical products in the Martian atmosphere (Clark et al., 2016). The weaker hydration signatures in spectra of the *purple patch* coatings compared to those of the *continuous coatings* we observed in the SuperCam VISIR data may also be consistent with this erosional hypothesis, as the longer surface exposure of the *purple patches* may have resulted in more water loss relative to the more recently exposed *continuous coatings*. The erosional hypothesis may also support the weaker ferric signatures observed in the Mastcam-Z data and more localized occurrences of thicker coatings only along Mure and Artuby Ridge, where steep exposures of the ridge and rock fractures have mitigated the impact of erosion and preserved the thick accumulations of indurated material confined to the sides and undersides of protruding rock layers.

Alternatively, the various expressions of coatings may represent grain size and compositional differences in the loose material that is being cemented. The less oxidized composition of the thicker coatings along Artuby ridge and Mure may suggest a more local contribution of the less ferric outcrops, which may have mechanically eroded to fill the fractures before cementation by local groundwater activity along fracture margins. *Purple patch* coatings, which exhibit the strongest ferric-like signatures, may include a higher percentage of ferric-rich airfall dust.

In addition, because the thicker coatings are confined to vertical surfaces, we cannot rule out a fluid-emplaced fracture fill origin for these particular features. For example, the thicker coatings may have resulted from enhanced fluid flow and dust/sediment accumulation within near-surface fractures along the geologic contact between the Máaz and Séítah formations. Alternative interpretations for the thicker features could include a wind polished agglutinated lava or some other unknown weathering phenomena. However, because of the textural and chemical similarities with the other coating classes described in this study, we favor the interpretation that such features represent surface coatings with potentially distinct erosional and/or formation histories.

4.2. Comparison With Rock Coatings at Previous Landing Sites

Rock coatings have previously been identified in situ at other landing sites and some of these features may be consistent with those observed in Jezero. At Gusev crater, the Mars Exploration Rover (MER) *Spirit* rover investigated a dark multilayer coating on basaltic rock target Mazatzal that was revealed following brushing and abrasion with the Rock Abrasion Tool (Arvidson et al., 2004; Haskin et al., 2005; McSween et al., 2004). Spectral and chemical analyses by *Spirit* instruments indicated that the coatings contained Fe-oxides, including crystalline hematite, and 2–5 times higher S and Cl concentrations relative to the rock interior (Haskin et al., 2005). The occurrence of the coatings on ventifact grooves suggested exposure to wind abrasion prior to coating formation, similar to the coatings observed at Jezero crater (Figure 16a). Previous studies hypothesized that the coatings on Mazatzal resulted from alteration of the silicate component of soil or of the rock itself, oxidation of Fe^{2+}, and incorporation of S and Cl (Haskin et al., 2005). Episodic burial and exhumation, along with transient liquid water provided by snow melt during periods of high obliquity or groundwater likely produced suitable alteration

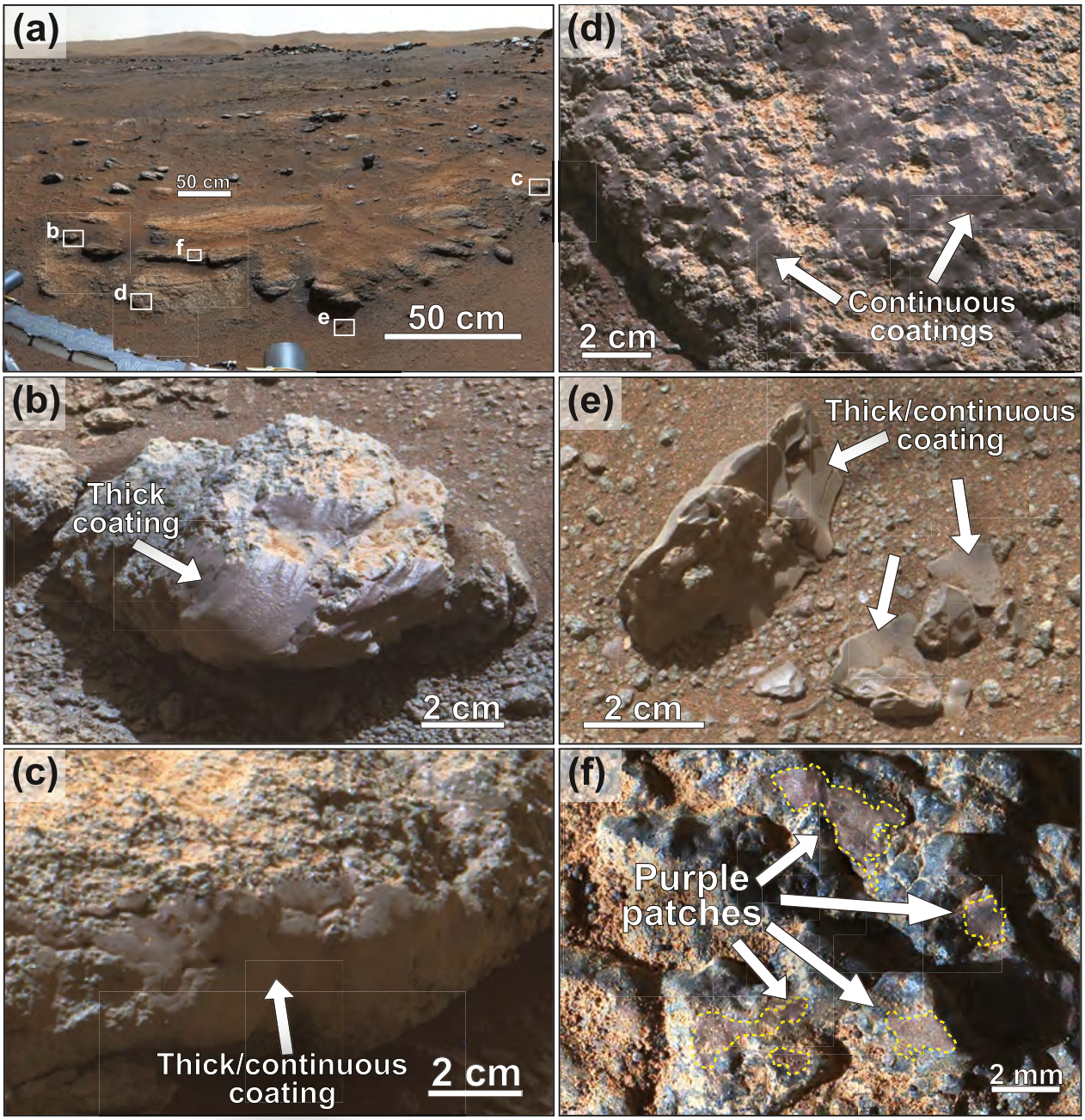

Figure 15. Various coating morphologies (white arrows) in the Rimplas workspace at the Artuby ridge, possibly illustrating an evolutionary pathway from thicker coatings to continuous coatings to purple patches. (a) Portion of Mastcam-Z left eye enhanced color Bayer filter mosaic (sol 343, zcam08371, Z34) for context. White boxes indicate location of images shown in (b–f). (b) Thick coating at Supercam target Taloire (sol 347, zcam08375, Z110). (c) Thick/continuous coating (sol 347, zcam08376, Z110). (d) Continuous coating at target Galabre (sol 345, zcam08372, Z110). (e) Eroded flakes at Mastcam-Z multispectral target Les Cluots (sol 346, zcam03315). (f) Purple patches (outlined in yellow dashed lines) at target Vergons as viewed by WATSON at 6 cm standoff (sol 345, srlc00378).

conditions for coating formation (Haskin et al., 2005). It is also possible that the surface coatings formed by weathering reactions without a condensed fluid phase during periods of high Martian humidity (McSween et al., 2004). Taken together, the composition and surface expressions of the coatings at Mazatzal suggest a formation mechanism similar to the coatings observed at Jezero.

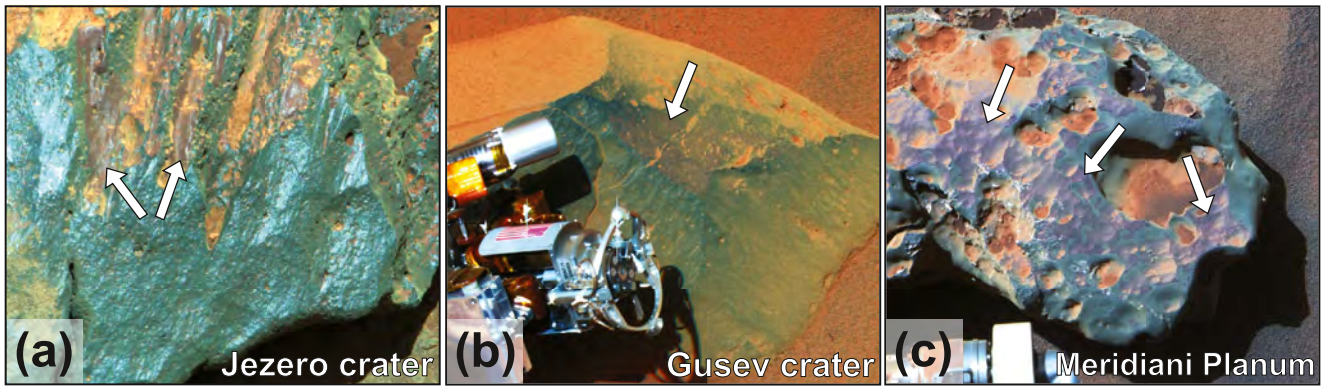

Figure 16. Comparison of rock coatings (white arrows) observed at Jezero and other landing sites. (a) Mastcam-Z L256 enhanced color image of Rochette (zcam03214, sol 188). (b) Spirit Panoramic Camera (Pancam) enhanced color (753 nm (L2), 535 nm (L5), and 432 nm (L7)) image of Adirondack (sol 30). (c) Opportunity Pancam L257 (same filter wavelengths as Spirit Pancam) enhanced color image of the Oileán Ruaidh meteorite (P2539, sol 2371).

Although obvious purple-hued coatings at the outcrop scale on Gusev plains rocks similar to those observed at Jezero have not been previously described, such coatings may be present in Gusev. The Adirondack rock, which is lithologically similar to the nearby Mazatzal and was also investigated by the *Spirit* rover, appeared to exhibit a discontinuous purple-hued patch on a higher standing wind abraded surface (Figure 16b). It is possible that this feature is consistent with the darker toned coatings investigated on Mazatzal and similar to the coatings observed at Jezero, but further investigation is needed to constrain any potential relationship.

At Meridiani Planum, the MER *Opportunity* rover observed discontinuous patches of purple-hued surface coatings on Fe-Ni meteorites (Figure 16c) (Ashley et al., 2011, 2022; Johnson et al., 2010; Schröder et al., 2008). Crosscutting relationships between the patches and meteorites confirmed that the surface features were not fusion crusts (Ashley et al., 2011, 2022). The patches typically occurred in topographically low areas and exhibited lobate margins that appeared to coat the underlying rock (Johnson et al., 2010). Pancam reflectance and Mössbauer data on the coatings suggested a mixture of ferric materials dominated by nanophase hematite. APXS data showed enrichment in Mg, Br, and Zn relative to the rest of the meteorite surface (Johnson et al., 2010). Previous studies hypothesized that these features represented an altered or secondary weathering coating, formed during episodes of burial and exhumation and partially eroded by subsequent wind abrasion. While it is possible these surface features resulted from iron-nickel-water interactions in the underlying meteorite, the *purple patches* may be consistent with those observed at Jezero crater and formed from induration and oxidation of externally derived material.

Further investigations by the *Opportunity* rover at Endeavour crater revealed an outcrop with a patchy, thin, dark, and likely mineralogically complex coating that was sulfate rich (~21 wt.%) with high abundances of Si, Fe, Ca, and Mg (Clark et al., 2016). The coating also contained an assemblage of Fe-oxides and/or oxyhydroxide phases, possibly including hematite, magnetite, goethite, and/or nanophase ferric oxides. Silicates were also present and included mafic minerals or amorphous materials, with a potential pyroxene source. Previous studies suggested that the coating composition could not solely be explained by soil or the amorphous component of soil with some added salts, and likely contained additional components that were indurated during coating formation (Clark et al., 2016). The compositional similarities between the coating observed at Endeavour crater and the Jezero coatings (e.g., sulfates, ferric oxides, silicates) may also suggest a similar origin, but further detailed chemical analyses are needed to constrain a potential shared formation mechanism. Veneers and thicker rinds were also identified by *Opportunity* rover on ancient sedimentary rocks at Meridiani Planum, but these features appeared morphologically distinct from the coatings described above and are hypothesized to have formed from precipitation of salts and interactions between the dust and the sulfate-rich outcrop surface (Farrand et al., 2007; Knoll et al., 2008). Other apparent coatings observed by *Opportunity* include dark Mn-rich surfaces on overturned rocks but were later interpreted to represent fracture fill material deposited by migrating fluids (Arvidson et al., 2016; Farrand et al., 2016).

The MSL *Curiosity* rover has been exploring sedimentary rocks within an ancient paleolake environment at Gale crater since August 2012. To date, reports of widespread surface coatings within Gale crater similar to those

observed by the *Perseverance* rover on the Jezero crater floor have not been documented in the published literature. However, more recent observations of some basaltic dark-toned float rocks likely derived from Gediz Vallis Ridge revealed an apparent surface coating that may be analgous to those observed at Jezero (Farrand et al., 2024; Garczynski et al., 2025). Dark surface features with high-Mn phases observed elsewhere by *Curiosity* were originally thought to be surface coatings that developed from modern chemical weathering processes, but subsequent studies determined that these features were more likely consistent with eroded diagenetic fracture fill (Lanza et al., 2016). Reported observations made by the Alpha Particle X-ray Spectrometer (APXS) indicated some chlorine enrichments that were interpreted to be associated with a surface rind rather than the bulk rock or dust (McCraig et al., 2020), though it remains unclear whether this rind is related to the surface coatings described in this study. Overall, the potential absence of widespread coatings in Gale crater and relative abundance on the Jezero crater floor is notable and warrants further investigation to better understand the factors influencing coating formation on Mars.

The observations of seemingly similar coatings observed by rovers elsewhere on Mars may provide important evidence that the coatings observed by the *Perseverance* rover are not unique to Jezero and likely represent a global Martian process. It is unclear whether these features are all associated with the same global alteration event or if they represent more local and distinct episodes of aqueous activity with similar formation mechanisms. We hypothesize that the common occurence of the rock coatings on the Jezero crater floor compared to other landing sites may be related one or a combination of factors including: (a) the relatively dust-free and dark-toned nature of the Jezero crater floor rocks making the coatings easier to identify at outcrop scale (Lasue et al., 2022; Tarnas et al., 2021), (b) distinct alteration conditions, (c) potentially more recent exhumation that has better preserved the coatings from long term erosion and removal by aeolian processes, or (d) the erosional resistance of the igneous bedrock. The erosional resistance hypothesis may help explain the occurrence of similar coatings on basaltic float rocks and Fe-Ni meteorites at other rover landing sites, and the absence of analogous coatings observed on sedimentary bedrock at Gale crater. The more stable nature of the igneous rocks and meteorites may have allowed more time for coatings to form and be preserved at the Martian surface relative to the more easily eroded and less stable sedimentary rocks at Gale.

4.3. Timing and Implications for Jezero Alteration History

The rock coatings described in this study provide key evidence of past alteration at Jezero and constraining the timing of coating formation will help further elucidate the geologic and alteration history of the crater. Observations of compositionally and morphologically similar surface coatings in both the Máaz and Séítah formations suggest that alteration conditions existed following the emplacement of both geologic units. Although the coatings were not observed on every rock investigated by the *Perseverance* rover during the Crater Floor Campaign, the relatively widespread nature of the rock coatings indicates surface alteration that affected the Jezero crater floor and possibly beyond. The presence of the coatings on eroded natural rock surfaces and ventifact grooves across the crater floor suggests that the most recent episode of coating formation occurred relatively late in the history of the crater, following exhumation and subsequent erosion of the crater floor rocks. Thus, the observed coatings on the crater floor may represent one of the last episodes of alteration activity at Jezero. The various coating morphologies and potential layering observed within some coatings may indicate multiple generations of coating formation, possibly representing distinct alteration events or periods of shallow burial and/or low abrasion rates. The patchy nature of some coatings indicates a period of ongoing erosion following deposition as the coatings are actively removed by aeolian abrasion. Additional work constraining a potential relationship of coating distribution with current and paleo-wind directions (Herkenhoff et al., 2023) may help elucidate the timing of coating deposition and erosion as well as past abrasion rates at Jezero (Kraft & Greeley, 2000).

While our study indicates that crater floor coatings likely represent alteration that occurred relatively late in the history of Jezero, it remains unclear when alteration conditions suitable for coating formation began and whether these conditions presently exist in the modern surface environment at Jezero. The evolution of the Jezero crater floor was likely complex and may have included multiple episodes of erosion, exhumation, and burial by an overlying unit on the order of tens of meters thick (Beyssac et al., 2023; Horgan et al., 2023; Quantin-Nataf et al., 2023). It is possible that coating formation occurred earlier during this complex history, but a record of those rock coatings has likely been erased by aeolian processes upon exposure. The occurrence of well-preserved *continuous coatings* on recently exposed lower lying rock surfaces may suggest active coating formation beneath

shallow regolith (Figure 7), possibly related to diurnal changes in relative humidity or potential frost events (Polkko et al., 2023). However, further research is needed to better understand whether coating formation is a modern process on Mars.

To further constrain the timing and implications of the rock coatings in the alteration history of Jezero, it is important to evaluate these features in the context of other evidence of alteration that has been observed on the crater floor. Previous studies have suggested that the Jezero crater floor was variably altered over multiple widespread alteration episodes. The relatively low proportion of hydrated alteration minerals detected within crater floor abrasion patches, combined with the lack of Al-phyllosilicates, suggested that these aqueous episodes involved limited water-rock interaction and duration (Beyssac et al., 2023; Clave et al., 2023; Farley et al., 2022; Mandon et al., 2023; Udry et al., 2023). Earlier stages of aqueous activity likely resulted in the formation of clay and carbonate minerals as a result of weathering of an Fe/Mg-bearing protolith in both the Máaz and Séítah formations. Subsequent alteration involving concentrated liquid brines, possibly associated with the evaporation of the Jezero paleolake, resulted in minor sulfate and perchlorate deposition within the pores of crater floor rocks (Mandon et al., 2023; Meslin et al., 2022). Because of the high solubility of these salts, it is hypothesized that these deposits may represent one of the last traces of fluid activity at Jezero crater. It is possible that the hydrated sulfates detected within the surface coatings were deposited during the same alteration event (Mandon et al., 2023; Meslin et al., 2022). Alternatively, the deposition and induration of surface coatings could have occurred in a separate and possibly later event that involved atmospheric-rock interactions at much lower water-rock ratios. Thus, further research is needed to constrain a potential relationship between the coatings and salts detected within the abraded patches.

Eroded flakes of coatings or coated rock fragments observed along the crater floor traverse are likely locally derived from nearby outcrops and may reflect the interplay between coating formation and weathering of the underlying rock (Figure 8). In particular, these features may be evidence of case hardening in which the downward mobilization of surface coating constituents into weathering rind pores created by mineral dissolution and mechanical fracturing hardens and protects the outer rock surface. Subsequent mineral dissolution beneath the case-hardened zone weakens the underlying rock, resulting in the detachment of coated rock flakes (Dorn et al., 2017). Weathering rinds have previously been inferred in coated rocks of both the Máaz (Horgan et al., 2023) and Séítah (Rice et al., 2023) formations, and further investigation is needed to understand the relationship and timing of coatings and alteration rinds on the Jezero crater floor.

As noted above, it is possible that the formation of soil crusts in Jezero crater may have occurred under similar aqueous conditions to the rock coatings. Previous studies at Jezero crater using the MEDA (Mars Environmental Dynamics Analyzer) instrument suggested diurnal adsorption of humidity into the ground and that frost conditions may have been achieved a few times during the *Perseverance* rover's investigations of the crater floor (Polkko et al., 2023). Water ice frost during nighttime at Jezero has also previously been predicted by climate models (Tamppari et al., 2022). While conditions favorable for soil crust formation may be possible on the present-day Martian surface, these conditions were more likely present in the recent past during periods of higher obliquity that were more suitable for frost formation to occur (Forget, 2009; Hausrath et al., 2023). It is plausible that the coatings described in this study formed concurrently with the soil crusts relatively late in the history of Jezero crater and likely share similar formation mechanisms. Shallow burial of bedrock by dust and fine regolith with low thermal inertia (Martínez et al., 2023) may have resulted in large diurnal changes in surface relative humidity that were suitable for the precipitation of salts and induration of surface coatings. Like soil crusts, the subsequent reworking and transport of eroded coatings may have contributed to younger generations of coatings as long as aqueous conditions persisted. Additional work focused on modeling past climates at Jezero may provide additional insight into past regolith-atmosphere interactions as well as the timing of soil crust and coating formation.

4.4. Future Investigations With Mars Sample Return

One of the key objectives of returned sample analysis is to characterize and better understand the water/rock/atmosphere interactions at the Martian surface through investigations of evidence for subaerial alteration. Rock coatings have previously been identified as a critical target for resolving the nature of past climatic and atmospheric conditions on Mars and identifying habitable environments that may have existed more recently in Mars' history (Beaty et al., 2019). Previous studies of rock coatings on Earth suggested that these sample targets may

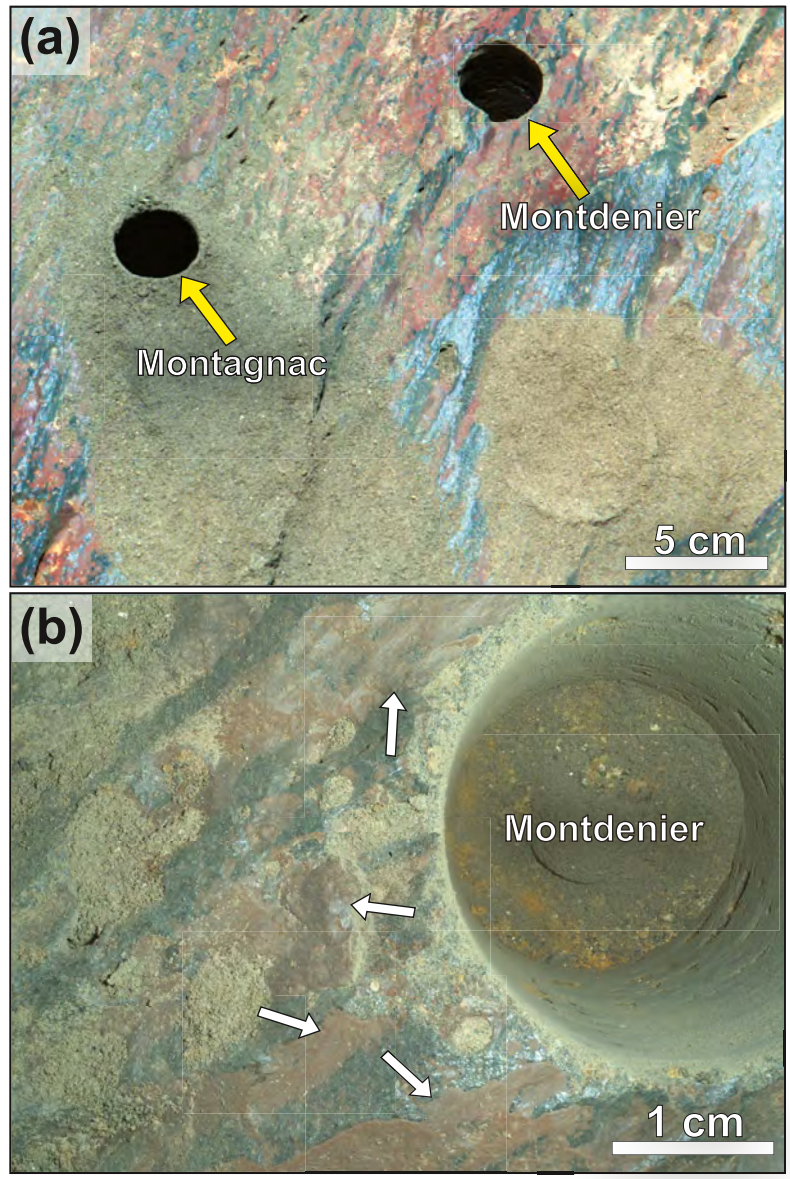

Figure 17. Rochette rock coatings (white arrows) potentially sampled by the Perseverance rover for Mars Sample Return. (a) Mastcam-Z L256 enhanced color image (sol 198 zcam03220, Máaz fm.) annotated with sampling locations (yellow arrows) and core names. (b) Focus merged WATSON image (sol 198 srlc08018) showing Montdenier borehole and nearby natural rock surface.

also have provided suitable habitats that protected microbes from harsh surface conditions, and thus are compelling for biosignature detection (Krinsley et al., 2009; Kuhlman et al., 2008; Wierzchos et al., 2013).

The *Perseverance* rover collected eight core samples from four scientifically return-worthy and representative rocks during the Crater Floor Campaign (Simon et al., 2023). Pairs of samples were collected from each rock so that one sample from each pair could be deposited in a "contingency" cache on the crater floor while the other half would be deposited in a primary cache along with samples collected by the rover on the delta and beyond Jezero. All crater floor rocks sampled by the Perseverance rover exhibited evidence of rock coatings described in this study; thus, it is possible that these surface features are included in the returned cache (Figure 17; Table 4). As shown in Figure S4 in Supporting Information S1, many of the pre-coring natural surfaces on sampled crater floor rocks appeared to exhibit *purple patch* coatings. These coatings were also evident on most of the natural surfaces

Table 4
Summary of Samples and Abrasion Patches From the Crater Floor Campaign Indicating the Occurrence of Natural Surface Coatings on Sampled Rocks

Sample name	Sol acquired	Abrasion	Formation	Coatings present on pre-coring surface? (See Figure S4 in Supporting Information S1)	Coatings present adjacent to abrasion patch? (See Figure S3 in Supporting Information S1)
Montdenier[a]	190	Bellegarde	Máaz	Yes	Yes
Montagnac	196	Bellegarde	Máaz	Yes	Yes
Salette	262	Dourbes	Séítah	Unclear due to dust cover	Yes
Coulettes[a]	271	Dourbes	Séítah	Yes	Yes
Robine	295	Quartier	Séítah	Yes	Unclear due to dust/tailings but present elsewhere on rock
Malay[a]	337	Quartier	Séítah	Unclear due to dust cover	Unclear due to dust/tailings but present elsewhere on rock
Hahonih	371	Alfalfa	Máaz	Yes	Yes
Atsah[a]	374	Alfalfa	Máaz	Yes	Yes

[a]Indicates samples included in the Three Forks contingency cache.

that were dust-cleared by nearby abrasion activities prior to sampling (Figure S3 in Supporting Information S1). While coatings were not obviously identified directly adjacent to the Quartier abrasion (likely obscured by abrasion tailings and/or dust), coatings were present elsewhere on the rock and thus may have been sampled (Figures 7b and 7e). It is unclear whether the coatings remained intact or were chipped off during the sample drilling process (Moeller et al., 2020). However, even if disturbed, it is likely that fragments of the coating were retained within the sample tube. Thus, any future sample curation efforts and investigations should look for the presence of these coatings within the crater floor sample tubes upon return to Earth.

If these coatings were successfully sampled, future laboratory analyses of these samples would be critical in helping answer outstanding questions presented in this work and further constrain the timing and nature of past alteration surface environments on Mars. In particular, detailed analyses could better assess the mineral, chemical, and isotopic compositions of the coatings that will allow for additional constraints on formation mechanisms, past Martian climate, and the potential relationship with other evidence of alteration. X-ray diffraction and conventional stable isotope techniques could be used to characterize bulk composition and determine the nature of the indurated material and source of reactant fluids within secondary alteration minerals (Simon et al., 2023). These results could be combined with nano- to microscale site-specific investigations using scanning electron microscopy, energy dispersive X-ray spectroscopy (EDS), synchrotron spectroscopy techniques, laser-ablation inductively coupled plasma mass spectrometry and secondary ion mass spectroscopy to characterize thickness and measure potential compositional and morphologic variability with depth and across different samples (Schindler & Dorn, 2017).

Laboratory data could help confirm whether coatings are layered from deposition over multiple generations as suggested in this study. If present, these microlaminations can record important paleoclimatic changes and help constrain the duration of water interaction as well as the chemistry, temperature, and residence time/drainage of the fluids (Beaty et al., 2019; Schindler & Dorn, 2017). Comparisons of these results with investigations of weathering rinds, salts preserved within the pores of crater floor bedrock, and components of soil crusts potentially contained within the regolith sample could help better assess whether these features are all related to one alteration event or distinct episodes late in the history of Jezero. In addition to characterizing past water activity, these analyses would also be important for the detection of ancient life that may have inhabited these coatings as mineral precipitates can preserve trapped organics and textural biosignatures (Beaty et al., 2019; Marnocha, 2017). These studies would also help inform our understanding of similar coatings observed at other landing sites, further elucidating the history of water at not only Jezero but also all of Mars.

5. Conclusions

In this work, we investigated the nature and origin of rock coatings observed by the *Perseverance* rover on the Jezero crater floor. In particular, we characterized the distribution, morphology, and texture of these surface features and presented results from Mastcam-Z and SuperCam spectral and chemical analyses to constrain the composition. Our analyses revealed that:

1. Rock coatings at Jezero crater are widespread and compositionally similar across the crater floor in both Máaz and Séítah formations and likely represent widespread surface alteration;
2. The occurrence of coatings on eroded and weathered natural surfaces suggests formation following recent exhumation and erosion of the crater floor, possibly representing the last episode of Jezero alteration activity;
3. Coatings are compositionally distinct and not correlated with underlying bedrock, suggesting formation through deposition and alteration of externally derived material;
4. The compositions of coatings are consistent with a variable mixture of airfall dust, potentially silt-sized regolith (<~21 μm grain size), and secondary alteration minerals such as iron oxides and sulfates, supporting previous water-rock-atmosphere interaction likely related to diurnal changes in relative humidity, frost events, meltwater, or other near surface aqueous activity;
5. The morphologies and "purpleness" of crater floor coatings are variable, which we hypothesize reflects various erosional expressions and/or different stages of coating evolution;
6. More *continuous coatings* occur on lower lying and recently exhumed surfaces, suggesting that shallow burial likely plays an important role in coating formation and/or subsequent preservation;
7. The crater floor coatings may be similar to coatings previously reported at other landing sites, suggesting a global alteration process that is not unique to Jezero. As at Jezero, coatings at other sites appear to occur on more durable or erosionally resistant rocks, highlighting the potential importance of physical rock properties in the formation and/or preservation of coatings. Coatings are more commonly observed at Jezero possibly reflecting unique formation or preservation conditions;
8. The *Perseverance* rover likely sampled these coatings during the Crater Floor Campaign, and future sample return studies should investigate these features to constrain past Martian climate and alteration activity, as well as search for biosignatures potentially preserved within coatings.

This study provides important context for future in situ rover investigations at Jezero and eventual sample return studies. Continued monitoring and characterization of rock coatings along the Perseverance rover's traverse may provide important insights into the extent and duration of past alteration activity as well as past erosional processes and the relative timing of crater exhumation. The results of this study may also have important implications for understanding past alteration and habitability beyond Jezero, as these coatings may be similar to those previously observed at other landing sites and may record some of the most recent alteration activity on Mars.

Data Availability Statement

The data in this publication are from the Mastcam-Z, SuperCam, and SHERLOC/WATSON instruments on the Mars 2020 Perseverance rover. All image data presented here from Mastcam-Z (Bell & Maki, 2021; https://doi.org/10.17189/q3ts-c749), SuperCam (Wiens & Maurice, 2021; https://doi.org/10.17189/1522646), and SHERLOC/WATSON (Beegle, 2021; https://doi.org/10.17189/1522643) are available through the Planetary Data System Imaging Node (https://pds-imaging.jpl.nasa.gov/portal/mars2020_mission.html) and GeoSciences Node (https://pds-geosciences.wustl.edu/missions/mars2020/). The Mastcam-Z multispectral database from sols 0-380 is published in Rice et al. (2022), which includes all Mastcam-Z spectra shown here. Software packages used for Mastcam-Z image processing, spectral extraction, and statistical analyses are part of the open source "marslab" suite by Million Concepts, LLC (St. Clair, 2022). The SuperCam major element oxide composition (MOC), total emissivity, and all raw data and processed calibrated data files are included in the Planetary Data System (Wiens & Maurice, 2021). A data set containing the full list of nearfield (<10 m away) and midfield (10–50 m away) rock targets used in this study, along with associated metadata data, is publicly archived and published in Garczynski (2025).

Acknowledgments
We thank the entire Mars 2020 science, operations, and engineering teams for making this work possible. Special thanks to the Mastcam-Z, SuperCam, and SHERLOC instrument teams for all their efforts in collecting the data presented in this work. We would also like to thank Mariek Schmidt and Bill Farrand for reviews that significantly improved the clarity of this paper. BG, BH, MR, JJ, JB, AV, JN, CM, MSC, AH, CT were funded by NASA's Mars 2020 Project via a subcontract from the California Institute of Technology/Jet Propulsion Laboratory to Arizona State University (subcontract 1511125). JJ was also funded through subcontracts through SuperCam via JPL (1532432). LM was supported by CNES, CNRS and IRIS OCAV. KK was supported by the Carlsberg Foundation Grant (CF19-0023). AB, GP, and CT were funded by ESA PRODEX Contract (PEA 4000117520) and FFG ASAP Contract 892662. EC was funded by the Canadian Space Agency (Grant 22EXPCO14) and the Natural Sciences and Engineering Research Council of Canada (Grant RGPIN-2021-02995). MM received funding from the E.U.'s Horizon 2020 research and innovation programme under the Marie Skłodowska-Curie Grant (801199). RCW was supported by JPL contract 46010000. AGF was supported by the European Research Council, Consolidator Grant 818602. MAS was supported by UK Space Agency Grants ST/V002732/1 and ST/V006134/1. CDKH was supported by Canadian Space Agency Mars 2020 Participating Scientist Grant CSA CGCPU 20EXPMARS. DF was funded by the Australian Research Council (Grant DE210100205).

References

Adams, J. B. (1975). Interpretation of visible and near-infrared diffuse reflectance spectra of pyroxenes and other rock-forming minerals. *Infrared and Raman spectroscopy of lunar and terrestrial minerals*, 91–116. https://doi.org/10.1016/B978-0-12-399950-4.50009-4

Anderson, R. B., Forni, O., Cousin, A., Wiens, R. C., Clegg, S. M., Frydenvang, J., et al. (2022). Post-landing major element quantification using SuperCam laser induced breakdown spectroscopy. *Spectrochimica Acta Part B: Atomic Spectroscopy*, *188*, 106347. https://doi.org/10.1016/j.sab.2021.106347

Arvidson, R. E., Anderson, R. C., Bartlett, P., Bell, J. F. III, Blaney, D., Christensen, P. R., et al. (2004). Localization and physical properties experiments conducted by spirit at Gusev Crater. *Science*, *305*(5685), 821–824. https://doi.org/10.1126/science.1099922

Arvidson, R. E., Squyres, S. W., Morris, R. V., Knoll, A. H., Gellert, R., Clark, B. C., et al. (2016). High concentrations of manganese and sulfur in deposits on Murray Ridge, Endeavour Crater, Mars. *American Mineralogist*, *101*(6), 1389–1405. https://doi.org/10.2138/am-2016-5599

Ashley, J. W., Golombek, M. P., Christensen, P. R., Squyres, S. W., McCoy, T. J., Schröder, C., et al. (2011). Evidence for mechanical and chemical alteration of iron-nickel meteorites on Mars: Process insights for Meridiani Planum. *Journal of Geophysical Research*, *116*(E7), E00F20. https://doi.org/10.1029/2010JE003672

Ashley, J. W., Herkenhoff, K. E., Schröder, C., Golombek, M. P., & the Athena Science Team. (2022). Topometric analysis of iron meteorite surfaces and their oxide coatings using microscopic imager digital elevation models at Meridiani Planum Mars—Support for recent equatorial mineral-water interaction and persistent paleowind direction. In *Proceedings of the 53rd lunar and planetary science conference (LPSC)*. Lunar and Planetary Institute. (abstract #1809).

Beaty, D. W., Grady, M. M., McSween, H. Y., Sefton-Nash, E., Carrier, B. L., Altieri, F., et al. (2019). The potential science and engineering value of samples delivered to Earth by Mars sample return. *Meteoritics & Planetary Sciences*, *54*(S1), S3–S152. https://doi.org/10.1111/maps.13242

Beegle, L. (2021). Mars 2020 SHERLOC bundle [Dataset]. *NASA Planetary Data System*. https://doi.org/10.17189/1522643

Bell, J. F., III, Godber, A., McNair, S., Caplinger, M. A., Maki, J. N., Lemmon, M. T., et al. (2017). The Mars Science Laboratory Curiosity rover Mastcam instruments: Preflight and in-flight calibration, validation, and data archiving. *Earth and Space Science*, *4*(7), 396–452. https://doi.org/10.1002/2016EA000219

Bell, J. F., III, & Maki, J. N. (2021). Mars 2020 Mast Camera Zoom Bundle, from Arizona State University Mastcam-Z Instrument Team, calibrated products [Dataset]. *NASA Planetary Data System*. https://doi.org/10.17189/q3ts-c749

Bell, J. F., III, Squyres, S. W., Herkenhoff, K. E., Maki, J. N., Arneson, H. M., Brown, D., et al. (2003). Mars exploration Rover Athena Panoramic camera (Pancam) investigation. *Journal of Geophysical Research*, *108*(E12), 8063. https://doi.org/10.1029/2003JE002070

Bell, J. F., Maki, J. N., Alwmark, S., Ehlmann, B. L., Fagents, S. A., Grotzinger, J. P., et al. (2022). Geological, multispectral, and meteorological imaging results from the Mars 2020 Perseverance rover in Jezero crater. *Science Advances*, *8*(47), eabo4856. https://doi.org/10.1126/sciadv.abo4856

Bell, J. F., Maki, J. N., Mehall, G. L., Ravine, M. A., Caplinger, M. A., Bailey, Z. J., et al. (2021). The Mars 2020 perseverance rover Mast Camera zoom (Mastcam-Z) multispectral, stereoscopic Imaging investigation. *Space Science Reviews*, *217*(1), 24. https://doi.org/10.1007/s11214-020-00755-x

Beyssac, O., Forni, O., Cousin, A., Udry, A., Kah, L. C., Mandon, L., et al. (2023). Petrological traverse of the olivine cumulate Séítah formation at Jezero crater, Mars: A perspective from SuperCam onboard perseverance. *Journal of Geophysical Research: Planets*, *128*(7), e2022JE007638. https://doi.org/10.1029/2022je007638

Bhartia, R., Beegle, L. W., DeFlores, L., Abbey, W., Razzell Hollis, J., Uckert, K., et al. (2021). Perseverance's scanning habitable environments with raman and luminescence for organics and chemicals (SHERLOC) investigation. *Space Science Reviews*, *217*(4), 58. https://doi.org/10.1007/s11214-021-00812-z

Bishop, J. L., Murchie, S. L., Pieters, C. M., & Zent, A. P. (2002). A model for formation of dust, soil, and rock coatings on Mars: Physical and chemical processes on the Martian surface. *Journal of Geophysical Research*, *107*(E11), 7-1–7-17. https://doi.org/10.1029/2001JE001581

Bridges, N. T., & Muhs, D. R. (2012). Duststones on Mars: Source, transport, deposition, and erosion. In *Sedimentary geology on Mars*.

Brown, A. J., Viviano, C. E., & Goudge, T. A. (2020). Olivine-carbonate mineralogy of the jezero Crater region. *Journal of Geophysical Research: Planets*, *125*(3), e2019JE006011. https://doi.org/10.1029/2019JE006011

Chide, B., Beyssac, O., Gauthier, M., Benzerara, K., Estève, I., Boulliard, J.-C., et al. (2021). Acoustic monitoring of laser-induced phase transitions in minerals: Implication for Mars exploration with SuperCam. *Scientific Reports*, *11*(1), 24019. https://doi.org/10.1038/s41598-021-03315-7

Clark, B. C., Morris, R. V., Herkenhoff, K. E., Farrand, W. H., Gellert, R., Jolliff, B. L., et al. (2016). Esperance: Multiple episodes of aqueous alteration involving fracture fills and coatings at Matijevic Hill, Mars. *American Mineralogist*, *101*(7), 1515–1526. https://doi.org/10.2138/am-2016-5575

Clavé, E., Benzerara, K., Meslin, P.-Y., Forni, O., Royer, C., Mandon, L., et al. (2023). Carbonate detection with SuperCam in igneous rocks on the floor of jezero crater, Mars. *Journal of Geophysical Research: Planets*, *128*(6), e2022JE007463. https://doi.org/10.1029/2022JE007463

Cloutis, E. A., & Gaffey, M. J. (1991). Pyroxene spectroscopy revisited: Spectral-compositional correlations and relationship to geothermometry. *Journal of Geophysical Research*, *96*(E5), 22809–22826. https://doi.org/10.1029/91JE02512

Cloutis, E. A., Gaffey, M. J., Jackowski, T. L., & Reed, K. L. (1986). Calibrations of phase abundance, composition, and particle size distribution for olivine-orthopyroxene mixtures from reflectance spectra. *Journal of Geophysical Research*, *91*(B11), 11641–11653. https://doi.org/10.1029/JB091iB11p11641

Dorn, R. I. (2009). Desert rock coatings. In A. J. Parsons & A. D. Abrahams (Eds.), *Geomorphology of desert environments* (pp. 153–186). Springer. https://doi.org/10.1007/978-1-4020-5719-9_7

Dorn, R. I., Mahaney, W. C., & Krinsley, D. H. (2017). Case hardening: Turning weathering rinds into protective shells. *Elements*, *13*(3), 165–169. https://doi.org/10.2113/gselements.13.3.165

Edgett, K. S., Caplinger, M., & Ravine, M. (2019). Mars 2020 perseverance SHERLOC WATSON camera pre-delivery characterization and calibration report. https://doi.org/10.13140/RG.2.2.18447.00165

Edgett, K. S., Caplinger, M. A., Maki, J. N., Ravine, M. A., Ghaemi, F. T., McNair, S., et al. (2015). Curiosity's robotic arm-mounted Mars Hand Lens Imager (MAHLI): Characterization and calibration status. In *Other report no. 0001; MSL MAHLI technical report, Volume 0001*. Mars Science Laboratory. https://doi.org/10.13140/RG.2.1.3798.5447

Edgett, K. S., Yingst, R. A., Ravine, M. A., Caplinger, M. A., Maki, J. N., Ghaemi, F. T., et al. (2012). Curiosity's Mars hand Lens imager (MAHLI) investigation. *Space Science Reviews*, *170*(1), 259–317. https://doi.org/10.1007/s11214-012-9910-4

Ehlmann, B. L., Mustard, J. F., Fassett, C. I., Schon, S. C., Head, J. W., III, Des Marais, D. J., et al. (2008). Clay minerals in delta deposits and organic preservation potential on Mars. *Nature Geoscience*, *1*(6), 355–358. https://doi.org/10.1038/ngeo207

Farley, K. A., Stack, K. M., Shuster, D. L., Horgan, B. H. N., Hurowitz, J. A., Tarnas, J. D., et al. (2022). Aqueously altered igneous rocks sampled on the floor of Jezero crater, Mars. *Science*, *377*(6614), eabo2196. https://doi.org/10.1126/science.abo2196

Farley, K. A., Williford, K. H., Stack, K. M., Bhartia, R., Chen, A., de la Torre, M., et al. (2020). Mars 2020 mission overview. *Space Science Reviews*, *216*(8), 142. https://doi.org/10.1007/s11214-020-00762-y

Farrand, W. H., Bell, J. F. III, Johnson, J. R., Arvidson, R. E., Crumpler, L. S., Hurowitz, J. A., & Schröder, C. (2008). Rock spectral classes observed by the Spirit Rover's pancam on the Gusev Crater Plains and in the Columbia Hills. *Journal of Geophysical Research*, *113*(E12), E12S38. https://doi.org/10.1029/2008JE003237

Farrand, W. H., Bell, J. F., III, Johnson, J. R., Jolliff, B. L., Knoll, A. H., McLennan, S. M., et al. (2007). Visible and near-infrared multispectral analysis of rocks at Meridiani Planum, Mars, by the Mars exploration Rover opportunity. *Journal of Geophysical Research*, *112*(E6), E06S02. https://doi.org/10.1029/2006JE002773

Farrand, W. H., Johnson, J. R., Rice, M. S., Wang, A., & Bell, J. F., III. (2016). VNIR multispectral observations of aqueous alteration materials by the Pancams on the spirit and opportunity Mars exploration Rovers. *American Mineralogist*, *101*(9), 2005–2019. https://doi.org/10.2138/am-2016-5627

Farrand, W. H., Trussell, A. R., Johnson, J. R., Bell, J. F., & Gasnault, O. (2024). Mastcam multispectral and Chemcam passive reflectance examination of dark-toned rocks from the stimson to upper Gediz Vallis Ridge in Gale Crater. In *Proceedings of the 55th lunar and planetary science conference (LPSC)*. Lunar and Planetary Institute. (abstract #2146).

Fassett, C. I., & Head, J. W., III. (2005). Fluvial sedimentary deposits on Mars: Ancient deltas in a crater lake in the Nili Fossae region. *Geophysical Research Letters*, *32*(14), L14201. https://doi.org/10.1029/2005GL023456

Forget, F. (2009). The present and past climates of planet Mars. In *EPJ web of conferences* (Vol. 1, pp. 235–248). https://doi.org/10.1140/epjconf/e2009-0924-9, EDP Sciences.

Fouchet, T., Reess, J.-M., Montmessin, F., Hassen-Khodja, R., Nguyen-Tuong, N., Humeau, O., et al. (2022). The SuperCam infrared spectrometer for the perseverance rover of the Mars2020 mission. *Icarus*, *373*, 114773. https://doi.org/10.1016/j.icarus.2021.114773

Garczynski, B. J. (2025). Coated and non-coated rock targets investigated by the perseverance rover on the floor of jezero crater, Mars [Dataset]. *Zenodo*. https://doi.org/10.5281/zenodo.15579706

Garczynski, B. J., Ollila, A. M., Johnson, J. R., Farrand, W. H., & Eng, A. O. (2025). Summary of rock coating observations on Mars from past rover missions. In *Proceedings of the 56th lunar and planetary science conference (LPSC)*. Lunar and Planetary Institute. (abstract #2769).

Gillespie, A. R., Kahle, A. B., & Walker, R. E. (1986). Color enhancement of highly correlated images. I. Decorrelation and HSI contrast stretches. *Remote Sensing of Environment*, *20*(3), 209–235. https://doi.org/10.1016/0034-4257(86)90044-1

Goudge, T. A., Head, J. W., Mustard, J. F., & Fassett, C. I. (2012). An analysis of open-basin lake deposits on Mars: Evidence for the nature of associated lacustrine deposits and post-lacustrine modification processes. *Icarus*, *219*(1), 211–229. https://doi.org/10.1016/j.icarus.2012.02.027

Goudge, T. A., Milliken, R. E., Head, J. W., Mustard, J. F., & Fassett, C. I. (2017). Sedimentological evidence for a deltaic origin of the western fan deposit in Jezero crater, Mars and implications for future exploration. *Earth and Planetary Science Letters*, *458*, 357–365. https://doi.org/10.1016/j.epsl.2016.10.056

Goudge, T. A., Mohrig, D., Cardenas, B. T., Hughes, C. M., & Fassett, C. I. (2018). Stratigraphy and paleohydrology of delta channel deposits, Jezero crater, Mars. *Icarus*, *301*, 58–75. https://doi.org/10.1016/j.icarus.2017.09.034

Haskin, L. A., Wang, A., Jolliff, B. L., McSween, H. Y., Clark, B. C., Des Marais, D. J., et al. (2005). Water alteration of rocks and soils on Mars at the Spirit rover site in Gusev crater. *Nature*, *436*, 7047. https://doi.org/10.1038/nature03640

Hausrath, E. M., Adcock, C. T., Bechtold, A., Beck, P., Benison, K., Brown, A., et al. (2023). An examination of soil crusts on the floor of jezero crater, Mars. *Journal of Geophysical Research: Planets*, *128*(10), e2022JE007433. https://doi.org/10.1029/2022JE007433

Hayes, A. G., Corlies, P., Tate, C., Barrington, M., Bell, J. F., Maki, J. N., et al. (2021). Pre-flight calibration of the Mars 2020 Rover Mastcam Zoom (Mastcam-Z) multispectral, stereoscopic imager. *Space Science Reviews*, *217*(2), 29. https://doi.org/10.1007/s11214-021-00795-x

Herkenhoff, K. E., Sullivan, R. J., Newman, C. E., Paar, G., Baker, M., Viúdez-Moreiras, D., et al. (2023). Comparison of ventifact orientations and recent wind direction indicators on the floor of jezero crater, Mars. *Journal of Geophysical Research: Planets*, *128*(3), e2022JE007599. https://doi.org/10.1029/2022JE007599

Horgan, B. H. N., Anderson, R. B., Dromart, G., Amador, E. S., & Rice, M. S. (2020). The mineral diversity of Jezero crater: Evidence for possible lacustrine carbonates on Mars. *Icarus*, *339*, 113526. https://doi.org/10.1016/j.icarus.2019.113526

Horgan, B. H. N., Johnson, J. R., Fraeman, A. A., Rice, M. S., Seeger, C., Bell, J. F., III, et al. (2020). Diagenesis of vera Rubin Ridge, gale crater, Mars, from mastcam multispectral images. *Journal of Geophysical Research: Planets*, *125*(11), e2019JE006322. https://doi.org/10.1029/2019JE006322

Horgan, B. H. N., Udry, A., Rice, M., Alwmark, S., Wiens, R. C., Bell, J. F., III, et al. (2023). Mineralogy, morphology, and emplacement history of the Maaz formation on the Jezero crater floor from orbital and rover observations. *Journal of Geophysical Research: Planets*, *128*(8), e2022JE007612. https://doi.org/10.1029/2022je007612

Jakosky, B. M., & Christensen, P. R. (1986). Global duricrust on Mars: Analysis of remote-sensing data. *Journal of Geophysical Research*, *91*(B3), 3547–3559. https://doi.org/10.1029/jb091ib03p03547

Johnson, J. R., Ashley, J., Bell, J. F., Farrand, W., & Yen, A. (2010). Surface alteration of Fe-Ni meteorites analyzed by the Opportunity Mars Exploration Rover. In *Goldschmidt conference (A473)*.

Johnson, J. R., Bell, J. F., Kinch, K. M., Merusi, M., Joseph, J., Rice, M., et al. (2022). Mastcam-Z spectrophotometric observations at the Van zyl overlook, jezero crater, Mars. In *Proceedings of the 53rd lunar and planetary science conference (LPSC)*. Lunar and Planetary Institute. (abstract #1253).

Kinch, K. M., Madsen, M. B., Bell, J. F., Maki, J. N., Bailey, Z. J., Hayes, A. G., et al. (2020). Radiometric calibration targets for the Mastcam-Z camera on the Mars 2020 rover Mission. *Space Science Reviews*, *216*(8), 141. https://doi.org/10.1007/s11214-020-00774-8

Knoll, A. H., Jolliff, B. L., Farrand, W. H., Bell, J. F., III, Clark, B. C., Gellert, R., et al. (2008). Veneers, rinds, and fracture fills: Relatively late alteration of sedimentary rocks at Meridiani Planum, Mars. *Journal of Geophysical Research*, *113*(E6), E06S16. https://doi.org/10.1029/2007JE002949

Kraft, M. D., & Greeley, R. (2000). Rock coatings and aeolian abrasion on Mars: Application to the pathfinder landing site. *Journal of Geophysical Research*, *105*(E6), 15107–15116. https://doi.org/10.1029/1999JE001229

Krinsley, D., Dorn, R. I., & DiGregorio, B. (2009). Astrobiological implications of rock varnish in Tibet. *Astrobiology*, *9*(6), 551–562. https://doi.org/10.1089/ast.2008.0238

Kuhlman, K. R., Venkat, P., La Duc, M. T., Kuhlman, G. M., & McKay, C. P. (2008). Evidence of a microbial community associated with rock varnish at Yungay, Atacama Desert, Chile. *Journal of Geophysical Research*, *113*(G4), G04022. https://doi.org/10.1029/2007JG000677

Lanza, N. L., Ollila, A. M., Cousin, A., Wiens, R. C., Clegg, S., Mangold, N., et al. (2015). Understanding the signature of rock coatings in laser-induced breakdown spectroscopy data. *Icarus*, *249*, 62–73. https://doi.org/10.1016/j.icarus.2014.05.038

Lanza, N. L., Wiens, R. C., Arvidson, R. E., Clark, B. C., Fischer, W. W., Gellert, R., et al. (2016). Oxidation of manganese in an ancient aquifer, Kimberley formation, Gale crater, Mars. *Geophysical Research Letters*, *43*(14), 7398–7407. https://doi.org/10.1002/2016GL069109

Lasue, J., Meslin, P. Y., Cousin, A., Forni, O., Anderson, R., Beck, P., et al. (2022). Comparison of dust between gale and jezero. In *Proceedings of the 53rd lunar and planetary science conference (LPSC)*. Lunar and Planetary Institute. (abstract #1758).

Lasue, J., Meslin, P. Y., Cousin, A., Forni, O., Anderson, R., Beck, P., et al. (2023). SuperCam first shots: Dust composition and variability. In *Proceedings of the 54th lunar and planetary science conference (LPSC)*. Lunar and Planetary Institute. (abstract #2806).

Legett, C., Newell, R. T., Reyes-Newell, A. L., Nelson, A. E., Bernardi, P., Bender, S. C., et al. (2022). Optical calibration of the SuperCam instrument body unit spectrometers. *Applied Optics*, *61*(11), 2967–2974. https://doi.org/10.1364/AO.447680

Lemmon, M. T., Smith, M. D., Viudez-Moreiras, D., de la Torre-Juarez, M., Vicente-Retortillo, A., Munguira, A., et al. (2022). Dust, sand, and winds within an active martian storm in jezero crater. *Geophysical Research Letters*, *49*(17), e2022GL100126. https://doi.org/10.1029/2022GL100126

Liu, Y., Tice, M. M., Schmidt, M. E., Treiman, A. H., Kizovski, T. V., Hurowitz, J. A., et al. (2022). An olivine cumulate outcrop on the floor of Jezero crater, Mars. *Science*, *377*(6614), 1513–1519. https://doi.org/10.1126/science.abo2756

Mandon, L., Quantin-Nataf, C., Royer, C., Beck, P., Fouchet, T., Johnson, J. R., et al. (2023). Reflectance of Jezero crater floor: 2. Mineralogical interpretation. *Journal of Geophysical Research: Planets*, *128*(7), e2022JE007450. https://doi.org/10.1029/2022JE007450

Mangold, N., Dromart, G., Ansan, V., Salese, F., Kleinhans, M. G., Massé, M., et al. (2020). Fluvial regimes, morphometry, and Age of jezero Crater Paleolake inlet Valleys and their exobiological significance for the 2020 rover Mission landing site. *Astrobiology*, *20*(8), 994–1013. https://doi.org/10.1089/ast.2019.2132

Mangold, N., Gupta, S., Gasnault, O., Dromart, G., Tarnas, J. D., Sholes, S. F., et al. (2021). Perseverance rover reveals an ancient Delta-Lake system and flood deposits at Jezero crater, Mars. *Science*, *374*(6568), 711–717. https://doi.org/10.1126/science.abl4051

Marnocha, C. L. (2017). Rock coatings and the potential for life on Mars. *Elements*, *13*(3), 187–191. https://doi.org/10.2113/gselements.13.3.187

Martínez, G. M., Sebastián, E., Vicente-Retortillo, A., Smith, M. D., Johnson, J. R., Fischer, E., et al. (2023). Surface energy budget, Albedo, and thermal inertia at jezero crater, Mars, as observed from the Mars 2020 MEDA instrument. *Journal of Geophysical Research: Planets*, *128*(2), e2022JE007537. https://doi.org/10.1029/2022JE007537

Maurice, S., Wiens, R. C., Bernardi, P., Caïs, P., Robinson, S., Nelson, T., et al. (2021). The SuperCam instrument suite on the Mars 2020 rover: Science objectives and mast-unit description. *Space Science Reviews*, *217*(3), 47. https://doi.org/10.1007/s11214-021-00807-w

McCraig, M. A., Gellert, R., Schmidt, M. E., Thompson, L. M., & Boyd, N. I. (2020). Chlorine enrichment at gale crater as investigated by APXS. In *Proceedings of the 51st lunar and planetary science conference (LPSC)*. Lunar and Planetary Institute. (abstract #2025).

McSween, H. Y., Arvidson, R. E., Bell, J. F., Blaney, D., Cabrol, N. A., Christensen, P. R., et al. (2004). Basaltic rocks analyzed by the Spirit rover in gusev crater. *Science*, *305*(5685), 842–845. https://doi.org/10.1126/science.3050842

Merusi, M., Kinch, K. B., Madsen, M. B., Bell, J. F., III, Maki, J. N., Hayes, A. G., et al. (2022). The Mastcam-Z radiometric calibration targets on NASA's perseverance rover: Derived irradiance Time-series, dust deposition, and performance over the first 350 sols on Mars. *Earth and Space Science*, *9*(12), e2022EA002552. https://doi.org/10.1029/2022EA002552

Meslin, P. Y., Forni, O., Beck, P., Cousin, A., Beyssac, O., Lopez-Reyes, G., et al. (2022). Evidence for perchlorate and sulfate salts in jezero crater, Mars, from SuperCam observations. In *Proceedings of the 53rd lunar and planetary science conference (LPSC)*. Lunar and Planetary Institute, United States of America. (abstract #2694).

Minitti, M. E., Kennedy, M. R., Edgett, K. S., Beegle, L. W., Asher, S. A., Abbey, W. J., et al. (2021). The Mars 2020 Watson imaging subsystem of the sherloc investigation and anticpated early results. In *53rd lunar and planetary science conference, the woodlands, TX*. Retrieved from https://ntrs.nasa.gov/citations/20220000131

Minitti, M. E., Weitz, C. M., Lane, M. D., & Bishop, J. L. (2007). Morphology, chemistry, and spectral properties of Hawaiian rock coatings and implications for Mars. *Journal of Geophysical Research*, *112*(E5), E05015. https://doi.org/10.1029/2006JE002839

Moeller, R. C., Jandura, L., Rosette, K., Robinson, M., Samuels, J., Silverman, M., et al. (2020). The sampling and caching subsystem (SCS) for the scientific exploration of jezero crater by the Mars 2020 perseverance rover. *Space Science Reviews*, *217*(1), 5. https://doi.org/10.1007/s11214-020-00783-7

Morris, R. V., Golden, D. C., Bell, J. F., Lauer, H. V., & Adams, J. B. (1993). Pigmenting agents in Martian soils: Inferences from spectral, Mössbauer, and magnetic properties of nanophase and other iron oxides in Hawaiian palagonitic soil PN-9. *Geochimica et Cosmochimica Acta*, *57*(19), 4597–4609. https://doi.org/10.1016/0016-7037(93)90185-Y

Morris, R. V., Lauer, H. V., Jr., Lawson, C. A., Gibson, E. K., Jr., Nace, G. A., & Stewart, C. (1985). Spectral and other physicochemical properties of submicron powders of hematite (α-Fe_2O_3), maghemite (γ-Fe_2O_3), magnetite (Fe_3O_4), goethite (α-FeOOH), and lepidocrocite (γ-FeOOH). *Journal of Geophysical Research*, *90*(B4), 3126–3144. https://doi.org/10.1029/JB090iB04p03126

Northup, D. E., Snider, J. R., Spilde, M. N., Porter, M. L., van de Kamp, J. L., Boston, P. J., et al. (2010). Diversity of rock varnish bacterial communities from Black Canyon, New Mexico. *Journal of Geophysical Research*, *115*(G2), 95. https://doi.org/10.1029/2009JG001107

Paar, G., Ortner, T., Tate, C., Deen, R. G., Abercrombie, P., Vona, M., et al. (2023). Three-dimensional data preparation and immersive mission-spanning visualization and analysis of Mars 2020 Mastcam-Z stereo image sequences. *Earth and Space Science*, *10*(3), e2022EA002532. https://doi.org/10.1029/2022EA002532

Parchert, K. J., Spilde, M. N., Porras-Alfaro, A., Nyberg, A. M., & Northup, D. E. (2012). Fungal communities associated with rock varnish in Black Canyon, New Mexico: Casual inhabitants or essential partners? *Geomicrobiology Journal*, *29*(8), 752–766. https://doi.org/10.1080/01490451.2011.619636

Perry, R. S., & Sephton, M. A. (2006). Desert varnish: An environmental recorder for Mars. *Astronomy and Geophysics*, *47*(4), 4.34–4.35. https://doi.org/10.1111/j.1468-4004.2006.47434.x

Polkko, J., Hieta, M., Harri, A.-M., Tamppari, L., Martínez, G., Viúdez-Moreiras, D., et al. (2023). Initial results of the relative humidity observations by MEDA instrument onboard the Mars 2020 perseverance rover. *Journal of Geophysical Research: Planets*, *128*(2), e2022JE007447. https://doi.org/10.1029/2022JE007447

Quantin-Nataf, C., Alwmark, S., Calef, F. J., Lasue, J., & Weiss, B. P. (2023). The complex exhumation history of jezero Crater floor unit and its implication for Mars sample return. *Journal of Geophysical Research: Planets*, *128*(6), e2022JE007628. https://doi.org/10.1029/2022JE007628

Rice, M. S., Bell, J. F., Cloutis, E. A., Wang, A., Ruff, S. W., Craig, M. A., et al. (2010). Silica-rich deposits and hydrated minerals at Gusev Crater, Mars: Vis-NIR spectral characterization and regional mapping. *Icarus*, *205*(2), 375–395. https://doi.org/10.1016/j.icarus.2009.03.035

Rice, M. S., Johnson, J., Million, C., Clair, M. S., Horgan, B., Vaughan, A., et al. (2022). Mastcam-Z multispectral database from the perseverance rover's traverse in the Jezero crater floor, Mars (sols 0-380) [Dataset]. *WWU Geology Faculty Publications*, *105*. https://doi.org/10.25710/bhyk-kc32

Rice, M. S., Johnson, J. R., Million, C. C., St. Clair, M., Horgan, B. N., Vaughan, A., et al. (2023). Spectral variability of rocks and soils on the Jezero crater floor: A summary of multispectral observations from Perseverance's Mastcam-Z instrument. *Journal of Geophysical Research: Planets*, *128*(10), e2022JE007548. https://doi.org/10.1029/2022JE007548

Royer, C., Fouchet, T., Mandon, L., Montmessin, F., Poulet, F., Forni, O., et al. (2023). Reflectance of jezero Crater floor: 1. Data processing and calibration of the infrared spectrometer (IRS) on SuperCam. *Journal of Geophysical Research: Planets*, *128*(1), e2022JE007481. https://doi.org/10.1029/2022JE007481

Salese, F., Kleinhans, M. G., Mangold, N., Ansan, V., McMahon, W., de Haas, T., & Dromart, G. (2020). Estimated minimum life span of the jezero fluvial Delta (Mars). *Astrobiology*, *20*(8), 977–993. https://doi.org/10.1089/ast.2020.2228

Salvatore, M. R., Mustard, J. F., Head, J. W., Cooper, R. F., Marchant, D. R., & Wyatt, M. B. (2013). Development of alteration rinds by oxidative weathering processes in Beacon Valley, Antarctica, and implications for Mars. *Geochimica et Cosmochimica Acta*, *115*, 137–161. https://doi.org/10.1016/j.gca.2013.04.002

Scheller, E. L., Razzell Hollis, J., Cardarelli, E. L., Steele, A., Beegle, L. W., Bhartia, R., et al. (2022). Aqueous alteration processes in Jezero crater, Mars—Implications for organic geochemistry. *Science*, *378*(6624), 1105–1110. https://doi.org/10.1126/science.abo5204

Schindler, M., & Dorn, R. I. (2017). Coatings on rocks and minerals: The interface between the lithosphere and the biosphere, hydrosphere, and atmosphere. *Elements*, *13*(3), 155–158. https://doi.org/10.2113/gselements.13.3.155

Schmidt, M. E., Allwood, A., Cable, M. L., Clark, B. C., Hausrath, E. M., Henneke, J., et al. (2024). Volcanic plume origin for widespread, indurated surface coatings in jezero crater. In *LPI Contributions, 3040*. (abstract 1954).

Schon, S. C., Head, J. W., & Fassett, C. I. (2012). An overfilled lacustrine system and progradational delta in Jezero crater, Mars: Implications for Noachian climate. *Planetary and Space Science*, *67*(1), 28–45. https://doi.org/10.1016/j.pss.2012.02.003

Schröder, C., Rodionov, D. S., McCoy, T. J., Jolliff, B. L., Gellert, R., Nittler, L. R., et al. (2008). Meteorites on Mars observed with the Mars Exploration Rovers. *Journal of Geophysical Research*, *113*(E6), E06S22. https://doi.org/10.1029/2007JE002990

Sherman, D. M., Burns, R. G., & Burns, V. M. (1982). Spectral characteristics of the iron oxides with application to the Martian bright region mineralogy. *Journal of Geophysical Research*, *87*(B12), 10169–10180. https://doi.org/10.1029/JB087iB12p10169

Simon, J. I., Hickman-Lewis, K., Cohen, B. A., Mayhew, L. E., Shuster, D. L., Debaille, V., et al. (2023). Samples collected from the floor of jezero crater with the Mars 2020 perseverance rover. *Journal of Geophysical Research: Planets*, *128*(6), e2022JE007474. https://doi.org/10.1029/2022JE007474

Smith, R. J., Horgan, B. H. N., Mann, P., Cloutis, E. A., & Christensen, P. R. (2017). Acid weathering of basalt and basaltic glass: 2. Effects of microscopic alteration textures on spectral properties. *Journal of Geophysical Research: Planets*, *122*(1), 203–227. https://doi.org/10.1002/2016JE005112

Stack, K. M., Williams, N. R., Calef, F., Sun, V. Z., Williford, K. H., Farley, K. A., et al. (2020). Photogeologic map of the perseverance Rover Field site in jezero crater constructed by the Mars 2020 science team. *Space Science Reviews*, *216*(8), 127. https://doi.org/10.1007/s11214-020-00739-x

St. Clair. (2022). MillionConcepts/marslab-reference: Initial release (v1.0.0) [Software]. *Zenodo*. https://doi.org/10.5281/zenodo.6642557

Sun, V. Z., Hand, K. P., Stack, K. M., Farley, K. A., Wogsland, B., Newman, C., et al. (2023). Overview and results from the Mars 2020 perseverance Rover's first science campaign on the jezero crater floor. *Journal of Geophysical Research: Planets*, *128*(6), e2022JE007613. https://doi.org/10.1029/2022je007613

Tamppari, L. K., Martinez, G., Manfredi, J. A. R., de la Torre-Juárez, M., Hieta, M., Polkko, J., & Lemmon, M. (2022). Relative humidity and vapor amount at Jezero Crater. In *Seventh international workshop on the Mars atmosphere: Modelling and observations* (p. 2305).

Tarnas, J. D., Mustard, J. F., Lin, H., Goudge, T. A., Amador, E. S., Bramble, M. S., et al. (2019). Orbital identification of hydrated silica in jezero crater, Mars. *Geophysical Research Letters*, *46*(22), 12771–12782. https://doi.org/10.1029/2019GL085584

Tarnas, J. D., Stack, K. M., Parente, M., Koeppel, A. H. D., Mustard, J. F., Moore, K. R., et al. (2021). Characteristics, origins, and biosignature preservation potential of carbonate-bearing rocks within and outside of Jezero Crater. *Journal of Geophysical Research: Planets*, *126*(11), e2021JE006898. https://doi.org/10.1029/2021JE006898

Tice, M. M., Hurowitz, J. A., Allwood, A. C., Jones, M. W. M., Orenstein, B. J., Davidoff, S., et al. (2022). Alteration history of Séítah formation rocks inferred by PIXL X-ray fluorescence, X-ray diffraction, and multispectral imaging on Mars. *Science Advances*, *8*(47), eabp9084. https://doi.org/10.1126/sciadv.abp9084

Udry, A., Ostwald, A., Sautter, V., Cousin, A., Beyssac, O., Forni, O., et al. (2023). A Mars 2020 perseverance supercam perspective on the igneous nature of the Máaz formation at Jezero crater and link with Séítah, Mars. *Journal of Geophysical Research: Planets*, *128*(7), e2022JE007440. https://doi.org/10.1029/2022JE007440

Vakkada Ramachandran, A., Zorzano, M.-P., & Martín-Torres, J. (2021). Experimental investigation of the atmosphere-regolith water cycle on present-day Mars. *Sensors*, *21*(21), 7421. https://doi.org/10.3390/s21217421

Vaughan, A., Minitti, M. E., Cardarelli, E. L., Johnson, J. R., Kah, L. C., Pilleri, P., et al. (2023). Regolith of the crater floor units, jezero crater, Mars: Textures, composition, and implications for provenance. *Journal of Geophysical Research: Planets*, *128*(3), e2022JE007437. https://doi.org/10.1029/2022JE007437

Viles, H. (1995). Ecological perspectives on rock surface weathering: Towards a conceptual model. *Geomorphology*, *13*(1), 21–35. https://doi.org/10.1016/0169-555X(95)00024-Y

Wang, A., Bell, J. F., III, Li, R., Johnson, J. R., Farrand, W. H., Cloutis, E. A., et al. (2008). Light-toned salty soils and coexisting Si-rich species discovered by the Mars exploration Rover spirit in Columbia Hills. *Journal of Geophysical Research*, *113*(E12), E12S33. https://doi.org/10.1029/2008JE003126

Wiens, R. C., & Maurice, S. (2021). Mars 2020 SuperCam bundle [Dataset]. *NASA Planetary Data System*. https://doi.org/10.17189/1522646

Wiens, R. C., Maurice, S., Barraclough, B., Saccoccio, M., Barkley, W. C., Bell, J. F., et al. (2012). The ChemCam instrument suite on the Mars Science Laboratory (MSL) Rover: Body unit and combined System tests. *Space Science Reviews*, *170*(1), 167–227. https://doi.org/10.1007/s11214-012-9902-4

Wiens, R. C., Maurice, S., Robinson, S. H., Nelson, A. E., Cais, P., Bernardi, P., et al. (2021). The SuperCam instrument suite on the NASA Mars 2020 rover: Body unit and combined system tests. *Space Science Reviews*, *217*, 1–87. https://doi.org/10.1007/s11214-020-00777-5

Wiens, R. C., Udry, A., Beyssac, O., Quantin-Nataf, C., Mangold, N., Cousin, A., et al. (2022). Compositionally and density stratified igneous terrain in Jezero crater, Mars. *Science Advances*, *8*(34), eabo3399. https://doi.org/10.1126/sciadv.abo3399

Wierzchos, J., Cámara, B., De Los Ríos, A., Davila, A. F., Sánchez Almazo, I. M., Artieda, O., et al. (2011). Microbial colonization of Ca-sulfate crusts in the hyperarid core of the Atacama Desert: Implications for the search for life on Mars. *Geobiology*, *9*(1), 44–60. https://doi.org/10.1111/j.1472-4669.2010.00254.x

Wierzchos, J., Davila, A. F., Artieda, O., Cámara-Gallego, B., de los Ríos, A., Nealson, K. H., et al. (2013). Ignimbrite as a substrate for endolithic life in the hyper-arid Atacama Desert: Implications for the search for life on Mars. *Icarus*, *224*(2), 334–346. https://doi.org/10.1016/j.icarus.2012.06.009

Wogsland, B. V., Minitti, M. E., Kah, L. C., Yingst, R. A., Abbey, W., Bhartia, R., et al. (2023). Science and science-enabling activities of the SHERLOC and WATSON imaging systems in jezero crater, Mars. *Earth and Space Science*, *10*(11), e2022EA002544. https://doi.org/10.1029/2022ea002544

Zastrow, A. M., & Glotch, T. D. (2021). Distinct carbonate lithologies in Jezero crater, Mars. *Geophysical Research Letters*, *48*(9), e2020GL092365. https://doi.org/10.1029/2020GL092365